



UPPSALA
UNIVERSITET

UPTec F 25049

Examensarbete 30 hp

Juni 2025

A Comparative Study of Integral Fuel Burnable Absorbers

Coupling Depletion and Fuel Performance

Oliver Kraft



UPPSALA
UNIVERSITET

A Comparative Study of Integral Fuel Burnable Absorbers: Coupling Depletion and Fuel Performance

Oliver Kraft

Abstract

Integral fuel burnable absorbers (IFBA) is a type of nuclear fuel developed by Westinghouse Electric Company that coats the fuel in a standard UO_2 fuel rod with ZrB_2 , a burnable absorber. IFBA is used for long term reactivity control, with it being especially useful for extended fuel cycles. ZrB_2 has many desirable material properties that make it suitable for IFBA. However, it predominantly captures neutrons through the $^{10}\text{B}(n,\alpha)$ reaction which produces helium. This helium leads to an elevated rod internal pressure (RIP), which becomes a safety concern at high burnup where fission gas release is also occurring. This thesis compares a range of alternatives to ZrB_2 with the goal of finding a material with similar performance, but lower helium production. To this end the depletion and fuel performance were compared for IFBA rods using a range of borides (ZrB_2 , DyB_6 , EuB_6 , YbB_6 , SmB_6 , HfB_2 , ErB_4) alongside cadmium oxide CdO . With regards to fuel performance, the differences were found to be negligible besides the difference in helium production and therefore RIP. It was concluded that the key metric for fuel performance in IFBA rods is the rod internal pressure. The depletion calculations demonstrated that two of the candidates ErB_4 and YbB_6 provided similar reactivity worths and lifetimes to ZrB_2 , but with the potential to reduce helium production. ErB_4 demonstrated higher potential in this regard, but both compounds were deemed to merit further investigation into manufacturability, cost and chemical compatibility. Additionally, the compounds GdB_6 and EuB_6 were found to have distinctly different depletion behaviours to ZrB_2 but could potentially be an interesting avenue for future research due to their high fraction of non-helium producing captures.

Teknisk-naturvetenskapliga fakulteten

Uppsala universitet, Utgivningsort Uppsala/Visby

Handledare: Kyle Johnson Ämnesgranskare: Vikram Rathore

Examinator: Tomas Nyberg

Populärvetenskaplig Sammanfattning

Atomkärnor består av två typer av partiklar, neutroner och protoner. Antalet protoner i en atomkärna avgör vilket grundämne atomen är, antalet neutroner avgör vilken isotop ("variant") av grundämnet. Neutroner är nyckeln som gör kärnreaktorer möjliga, när vissa tunga atomkärnor träffas av en neutron klyvs de i en reaktion som kallas för fission. I processen frigörs stora mängder energi och ett antal nya neutroner produceras. De nya neutronerna kan användas för att orsaka vidare fissionsreaktioner, som kan orsaka ytterligare reaktioner i en självdrivande kedjereaktion. Energin som frigörs vid fission konverteras i kärnkraftverk till värme som sedan används för att producera elektricitet.

Denna rapport fokuserar på så kallade lättvattenreaktorer, dessa är konstruerade kring en tank med vatten fylld med bränslestavar arrangerade i ett rutnät. Bränslestavarna är i sin tur slutna rör bestående av en zirkoniumlegering som omsluter en stapel med cylindriska bränslepellets. Utöver bränsle innehåller reaktorer neutron absorberande material för att kontrollera kedjereaktionen. Dessa material finns exempelvis i styrstavar som kan sättas in för att styra effekten på reaktorn. När neutroner blir fångade i material som inte kan genomgå fission stoppas de från att bidra till kedjereaktionen, vilket sänker energiproduktionen i reaktorn.

Utöver styrstavar används förbränningsbara absorbatörer för att passivt begränsa effekten i reaktorer. Som namnet antyder är dessa ämnade att konsumeras, förbrännas, medans de fångar in neutroner. De används för att minska behovet av aktiv styrning med till exempel styrstavar, särskilt i början av bränslecykeln när bränslet annars är svårare att styra. Förbränningsbara absorbatörer finns i många olika former, en av dem är Integral Fuel Burnable Absorber (IFBA) en typ av bränsle utvecklat av Westinghouse. IFBA inkluderar ett ytbelägg på bränslet inuti bränslestavarna som är applicerat direkt på bränslet.

Detta examensarbete presenterar datorsimuleringar för att jämföra alternativa material som kan användas till ytskiktet i IFBA stavar för att försöka hitta något som kan förbättra prestandan. I dagsläget används zirkonium diborid (ZrB_2) för ytskiktet, detta har använts med framgång i många år eftersom det har en relativt låg kostnad, bra materialegenskaper och en förbrukningstakt som passar bra för användningsområdet. Detta material har dock en stor nackdel, när ZrB_2 fångar in neutroner produceras helium. Detta är problematiskt, eftersom bränslestavar är slutna så leder detta helium till en tryckbildning inuti bränslestaven. Blir trycket för högt så kommer bränslestaven svälla som likt en ballong, och sedan spricka. Bränslestavar är designade för att vara förseglade för att hålla det mycket radioaktiva bränslet samlat och säkrare att hantera.

För detta arbete studerades ett antal olika material som har liknande kemiska egenskaper till ZrB_2 . Till skillnad från ZrB_2 , så inkluderar de

studerade materialen dock neutron absorberande isotoper som inte producerar helium. Förhoppningen var att de på grund av detta borde kunna ha en liknande effekt på reaktorn men med mindre heliumproduktion. Olika material är dock olika benägna att fånga in neutroner. För att jämföra de studerade materialen gjordes därför simuleringar som undersökte hur snabbt de olika ämnena konsumeras, hur de påverkade reaktorn och hur de påverkade bränslestavarna.

Resultatet av detta var att två ämnen, erbium tetraborid (ErB_4) och ytterbium hexaborid (YbB_6), visade sig ha liknande prestanda till ZrB_2 . En markant andel av de infångade neutronerna i båda material producerade dock inte helium. Båda verkar därför lovande och kan ha potential som direkta ersättare till ZrB_2 . Framtida studier behövs dock för att undersöka t.ex. deras kemi så att de går att producera till en rimlig kostnad, och att de inte har några kemiska reaktioner med andra material i bränslestaven som kan utgöra en säkerhetsrisk.

Ytterligare två av de studerade ämnena (GdB_6 och EuB_6) var markant starkare absorbatörer än ZrB_2 , och en ännu större andel infångade neutroner som inte producerade helium. De hade dock väldigt annorlunda livslängd jämfört med ZrB_2 , det är lite oklart om deras livslängd är användbar för dagens reaktorer. Det skulle behövas mer detaljerade simuleringar än vad som var möjliga här för att avgöra om de kan vara till nytta som IFBA ytbelägg, men de presenterar en intressant vinkel för framtida forskning.

Contents

1	Introduction	3
1.1	Burnable Absorbers	4
1.2	Aims	6
1.3	Limitations	7
2	Background	8
2.1	Neutron reactions & Interactions	8
2.1.1	Scattering	9
2.1.2	Capture & Absorption	9
2.1.3	Fission	10
2.2	Reactor Theory	10
2.2.1	Neutron Transport	11
2.2.2	Criticality	13
2.2.3	Solving the Transport Problem	14
2.2.4	Burnup & Depletion	15
2.2.5	Solving The Burnup Problem	16
2.2.6	Core Loading & Fuel Management	17
2.3	Types of Nuclear Reactors	17
2.3.1	Pressurised Water Reactors	18
2.3.2	Boiling Water Reactors	19
2.4	LWR Fuel	21
2.4.1	Evolution During Burnup	21
2.4.2	High Burnup Structure	22
2.4.3	Fuel Fragmentation, Relocation and Dispersal	23
2.5	Burnable Absorbers	23
2.5.1	Integral Burnable Absorbers	25
2.5.2	Integral Fuel Burnable Absorbers	25
2.6	Overview of Candidate Coatings	26
3	Methodology	28
3.1	Neutronics	28
3.1.1	Criticality Calculation Parameters	31
3.1.2	Burnup Calculation Parameters	32

3.1.3	Output Parameters & Post-Processing	34
3.2	Transuranus Setup	35
3.2.1	Fuel Rod Characteristics	36
3.2.2	Conversion of Serpent Results	37
3.2.3	Modelling IFBA Gas Production	38
4	Results	40
4.1	Neutronics	40
4.1.1	Capture rate & ^4He Production	43
4.1.2	Local Effects in Fuel	45
4.1.3	Xenon Concentration	47
4.1.4	Uranium-235 and Plutonium-239 Concentration	47
4.2	Fuel Performance	50
4.2.1	Power History Sensitivity Analysis	50
4.2.2	Radial Power Profile Validation	51
4.2.3	IFBA Gas Release Validation	52
4.2.4	Results for Alternative IFBA Compounds	53
5	Discussion	57
5.1	Neutronics of IFBA and IBA	57
5.2	Neutronics of Alternative IFBA Coatings	58
5.2.1	ErB_4 , YbB_6 and DyB_6	59
5.2.2	GdB_6 , SmB_6 and CdO	60
5.2.3	EuB_6	60
5.2.4	ZrB_2^* and HfB_2^*	61
5.3	Transuranus Simulation Accuracy	61
5.3.1	Power History Sensitivity & Fission Gas Release	62
5.3.2	Radial Power Profile	62
5.3.3	IFBA Gas Release	63
5.4	Fuel Performance of Alternative IFBA Coatings	63
5.5	Key Insights & Outlook for IFBA Development	64
6	Conclusion	67
6.1	Acknowledgments	68
A	Appendix	73
A.1	Total Fission Rate	74
A.2	Uranium-235 Fission Rate	76
A.3	Uranium-238 Capture Rate	78

Chapter 1

Introduction

Nuclear energy plays a critical role in supplying electricity in many countries around the world, and about 10 % of electricity globally comes from nuclear power plants. [27] With the transition towards low carbon energy sources it is becoming increasingly important as well. Nuclear energy is a useful complement to renewables and can serve to cover the baseload, the non-varying part of our electricity usage. With renewables such as wind, solar and hydropower covering the remainder.

Nuclear energy utilizes the energy released from the nuclear fission reaction. Fission is a process which certain heavy nuclei undergo when capturing a neutron resulting in the splitting of said nucleus. In the process a large amount of energy is released and a number of new neutrons are produced. Because neutrons are used to induce and produced during fission it is possible to create a self-sustaining chain reaction where in one fission reaction induces another which induces another, and so on. This is what is utilized in nuclear power plants, this creates a continuous source of heat which is used to produce steam, driving a turbine connected to a generator to produce electricity. [16]

Various designs exist for nuclear reactors, the focus of this thesis is however on light water reactors (LWRs). In an LWR the core is typically constructed as an array of rectangular assemblies submerged in water. Each fuel assembly is in turn made up of an array of cylindrical fuel rods. Alongside these the reactor typically contains various means of reactivity control such as fuel rods, boric acid in the water or burnable absorbers. The goal in reactivity control is to ensure the nuclear chain reaction remains controlled. The aforementioned methods achieve this by introducing neutron absorbers into the core, these capture some neutrons preventing them from reaching the fuel and propagating the chain reaction. This reduces the fission rate, and thereby the neutron production rate. A more detailed description of two types of LWR reactors will follow in section 2.3.

Figure 1.1 shows a simplified illustration of a nuclear fuel rod highlighting

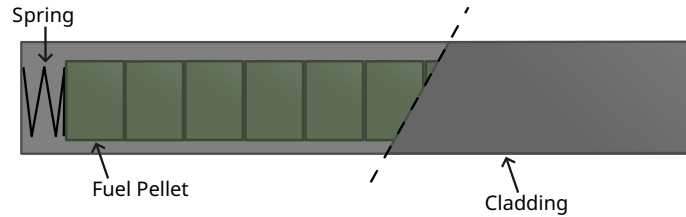


Figure 1.1: An illustration of a fuel rod showing a partial cross-section with annotations marking the plenum spring, the fuel pellets and the cladding. Note that the figure is not to scale.

the most important regions. A fuel rod is typically around 4 metres in height and 1 centimetre in diameter. The outer surface is the cladding, typically made of a zirconium alloy such as zircalloy. Inside the fuel rod there is then a small void separating the cladding from a stack of fuel pellets, typically made up of UO_2 , but could also be a uranium-plutonium oxide mixture (MOX). At the top of the fuel rod there is also a void, a plenum, to allow for the release of fission gases without excessive pressure build up. There is also a spring in the plenum which keeps the fuel pellets held in place. [1]

A challenge in operating a reactor is that refuelling is costly and time-consuming often requiring the reactor to be shut down for extended periods of time. For this reason reactor operators want to use the fuel for as long as possible. However, as fuel is used in a reactor it is depleted, the fissile nuclei in the fuel are consumed reducing the reactivity of the fuel over time. Depletion, or burnup, is typically measured in MWd/kgU , i.e. amount of extracted energy per initial kilogram of uranium in the fuel which is proportional to the number of cumulative number of fission events.

Today nuclear reactor operators are moving from 12 to 18 or even 24 month fuel cycles, the time between refuelling the reactor. These extended fuel cycles are exposing the fuel to increasing burnup, moving from 50-60 MWd/kgU towards 70+ MWd/kgU . Maintaining reactivity margins to keep the chain reaction self-sustaining at such high burnup necessitates high initial enrichment of the fuel, which in turn leads to high initial reactivity. This can pose controllability challenges, but also increases the risk of local power peaking in the reactor core. These challenges have lead reactor operators to pursue burnable absorbers to a larger extent as they can counteract these challenges with fresh fuel very effectively. [8]

1.1 Burnable Absorbers

Burnable absorbers (BA) are materials introduced into a reactor which capture neutrons, reducing the flux and therefore power. However, in contrast

to e.g. control rods which contain large enough amounts of absorbent material to essentially not deplete, burnable absorbers contain only a small amount such that the burnable absorber is entirely consumed, “burned”. This can be used to counteract the increased reactivity of higher enrichment in the beginning of a fuel cycle, whilst keeping the beneficial increased reactivity towards the end. [29] Burnable absorbers can take many forms such as full absorber rods, rods with an homogenous mixture of fuel and a burnable poison (IBA), integral fuel burnable absorbers (IFBA), along with some more exotic alternatives; IFBA being the focus of this thesis. [7]

IBA is by far the most common type of burnable absorber, with gadolinia (Gd_2O_3) being a particularly popular BA to mix into the fuel. However, erbia (Er_2O_3) also sees some limited use, though significantly less due to its higher cost. Aside from the pellets inside the rod being a homogeneous mixture of BA and fuel the rods are otherwise identical to regular fuel rods as shown in figure 1.1.

IFBA is a product developed by Westinghouse Electric Company which takes a normal UO_2 fuel rod and adds a burnable absorber coating directly to the fuel. The burnable absorber in IFBA rods is only on the periphery of the fuel pellets. [7] Presently Westinghouse uses zirconium diboride (ZrB_2) for the coating in its IFBA rods. This introduces challenges, because the coating is applied inside the sealed fuel rod any gas produced as the coating is depleted will lead to a pressure increase. Pressures are already a significant safety consideration in standard fuel at high burnup without additional gas pressure, mainly due to the release of gaseous fission products from the fuel.

Unfortunately, with ZrB_2 the only notable neutron absorption reaction is:



This reaction produces helium which is released into the free volume in the fuel rod. This leads to an increase in rod internal pressure that must be managed as it can reduce safety margins and threaten cladding integrity. Presently this is done by reducing fill gas pressure and removing fuel, the latter being especially undesirable.

Recent post-irradiation examination of IFBA rods has indicated potentially desirable benefits thought to be related to the flattening of the radial power profile. Further work is required to validate these results before they can be made public, this effect is therefore not a focus of this thesis. The focus will be on alternative IFBA candidates that are less reliant on equation (1.1), thereby reducing the increase in internal pressure as the absorber is consumed.

IFBA has seen extensive use in the United States, where it is typically used in conjunction with other burnable absorbers in pressurized water reactors. As of 2018 over 4 million IFBA rods had been produced, with interest increasing due to the aforementioned pursuit for longer fuel cycles.

[31] Presently IFBA has not been introduced on the European market, with European operators generally favouring IBA for fuel integrated burnable absorbers.

1.2 Aims

To state the aim of this project more concretely, the goal is to find an alternative to ZrB_2 that gives better or similar depletion characteristics with lower helium production. In general the desirable characteristics of a burnable absorber can be summarized as the following:

- Reduction of beginning of cycle (BOC) reactivity.
- A lifetime in the fuel of 10-20 MWd/kgU, preferably tunable
- Zero or very low end of cycle (EOC) reactivity penalty.
- Maintain similar or improve fuel performance to ZrB_2 IFBA, mainly the helium contribution to rod internal pressure (RIP)

Using simulations these characteristics were investigated for a range of different compounds and compared to ZrB_2 . Depletion calculations were performed using the neutron transport code Serpent 2, the results of these calculations were then used in the fuel performance code Transuranus. It should be noted that due to the resources available it was not feasible to perform parameter optimisation, “tunability” will therefore only be touched upon theoretically in the context of key physics and depletion characteristics.

The studied compounds include the currently used ZrB_2 , alongside alternative borides and one boron-free oxide. Specifically, the studied compounds are the following:

- ZrB_2
- GdB_6
- DyB_6
- EuB_6
- YbB_6
- SmB_6
- HfB_2
- ErB_4
- CdO

The candidates were selected with a goal of obtaining similar chemical properties to ZrB_2 to decrease the likelihood of a chemical incompatibility with either fuel or cladding, and allow for similar application techniques. Most of the considered compounds are therefore still borides. The only non-boride tested is CdO , its applicability is less certain because of this,

and it does have known interactions with zirconium. However, its neutron cross-section still makes it an interesting candidate to explore. [9, 25]

1.3 Limitations

Aside from focusing on chemically similar compounds to ZrB_2 , manufacturability and chemical compatibility have not been considered in the candidate selection. Any identified compound of interest would require further investigation to establish its applicability because of this.

Additionally, the extensive computational time required for depletion calculations also imposed some limitations. In the time available it was not feasible to study the impact of varying the thickness or other parameters such as isotopic composition. Detailed studies on a parameter level will be left for future studies, possibly using the results obtained here to narrow down the selection of studied compounds.

Chapter 2

Background

This chapter describes the necessary theory and background required to understand the present work. For the unfamiliar reader, a short description of neutron physics and reactor theory will first be given. This will be followed by a description of different types of nuclear reactors, light water reactor fuel and burnable absorbers. Finally, an overview of the considered candidates will be given.

2.1 Neutron reactions & Interactions

The neutron and its interactions are key for nuclear reactors. It is an electrically neutral particle which only interacts through the strong force, this makes their motion very simple. Neutrons travel in straight lines, only deviating from their straight line through collisions with nuclei. [17]

The likelihood of an interaction is described using cross-sections σ , measured in barns ($1 \text{ b} = 10^{-28} \text{ m}^2$). The cross-section describes the probability of a single neutron interacting with a nucleus, it essentially describes the cross-sectional area of the nucleus. It is dependent on both the temperature of the material and the kinetic energy of the neutron. The best way to understand cross-sections is through how it relates to the reaction rate:

$$R = N\sigma\phi \quad (2.1)$$

where R is the reaction rate for some reaction, N is the number of nuclei with microscopic cross-section σ and neutron flux ϕ . A related term is the macroscopic cross-section Σ :

$$\Sigma = n\sigma \quad (2.2)$$

where n is the number density. The macroscopic cross-section describes the mean distance between interactions. [17]

2.1.1 Scattering

Scattering is the simplest possible neutron interaction. It is an interaction wherein a neutron "bounces" against a nucleus, in the process it will lose some kinetic energy to the nucleus and be redirected. The amount of energy lost in each scattering interaction is usually relatively small, however, scattering cross-sections are quite high and therefore scattering tends to occur a lot. [17, 6]

2.1.2 Capture & Absorption

Another notable category of neutron reactions is capture and absorption. These are reactions in which the incident neutron is lost through an interaction with a nucleus. A distinction is made here with capture reactions being reactions that produce no secondary neutron, and absorption reactions being reactions where merely the incident neutron is lost (i.e. all capture + fission). [16] Fission reactions will be described in the next section.

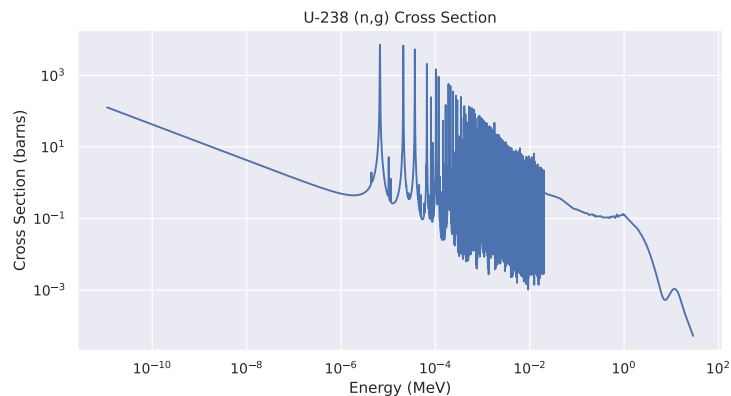


Figure 2.1: The figure shows the cross-section for the ${}^{238}\text{U}(n, \gamma)$ reaction as a function of incident neutron energy.

Capture reactions are reactions such as equation (1.1) or (2.3) where a nucleus absorbs a neutron. This results in the loss of both the incident neutron and the transmutation of the capturing nucleus. The cross-section as for the ${}^{238}\text{U}(n, \gamma)$ reaction is shown in figure 2.1, highlighting the previously described energy dependence of the cross-section.

Capture reactions are used to control the neutron population by stopping neutrons from causing fission reactions. This makes them useful for controlling the power. Capture reactions are the reason e.g. control rods, or burnable absorbers (described in more detail in section 2.5) work. [16]

Capture reactions also need to be considered when selecting materials for reactors as, e.g. steel, has quite high capture cross-sections. This makes it unsuitable for use in high flux regions as its properties change due to transmutation under irradiation, which can lead to significant changes in the material and potentially pose a safety risk. [16]

2.1.3 Fission

When some heavy nuclei, such as uranium-235, capture a neutron they undergo fission. Fission is a nuclear reaction which splits the nucleus into two (or in rare cases more) fission products. This reaction produces a large amount of energy, approximately 200 MeV, and 2-6 neutrons. The fission energy is predominantly released as kinetic energy of the fission fragments, with some energy going to the neutrons released and a small amount going to gamma rays. [17]

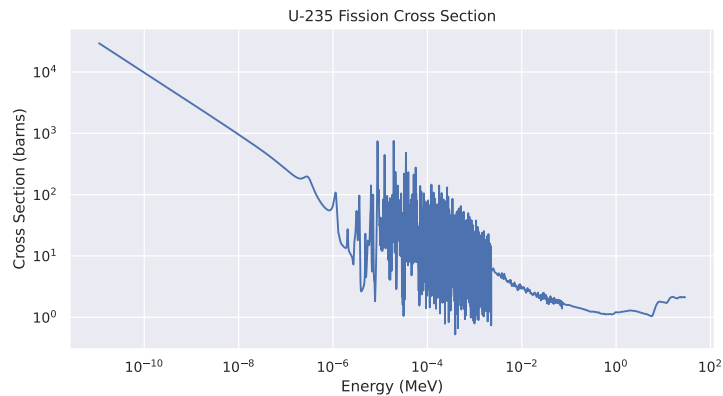


Figure 2.2: The figure shows the fission cross-section of ^{235}U as a function of incident neutron energy.[2]

The fission cross-section for the isotope uranium-235 is shown as a function of energy in figure 2.2. The notable features of this plot is the inverse proportionality to neutron energy at low energies and the peak structure at intermediate energies. The inverse proportionality indicates that to maximize the fission rate it is desirable to minimize the neutron energy, this is a concept utilized in reactors operating in the so-called thermal spectrum. The peaks seen at higher energies are resonance peaks, these arise due to the internal energy structure of the fissioning nucleus.

2.2 Reactor Theory

Nuclear reactors are built around the key fact that only a single neutron is required to induce fission but more than one neutron is produced. The

neutrons released from one fission reaction can initiate new fission reactions, releasing additional neutrons, causing further fission reactions, and so on. This process is called a chain reaction, and it is illustrated in figure 2.3. Whether a chain reaction is possible or not largely depends on the properties of the geometry of the system and the materials involved. Neutrons may be sent out of the fissile material and lost or captured by other non-fissile nuclei. If this happens at a higher rate than neutrons are produced from fission a chain reaction cannot be self-sustaining.

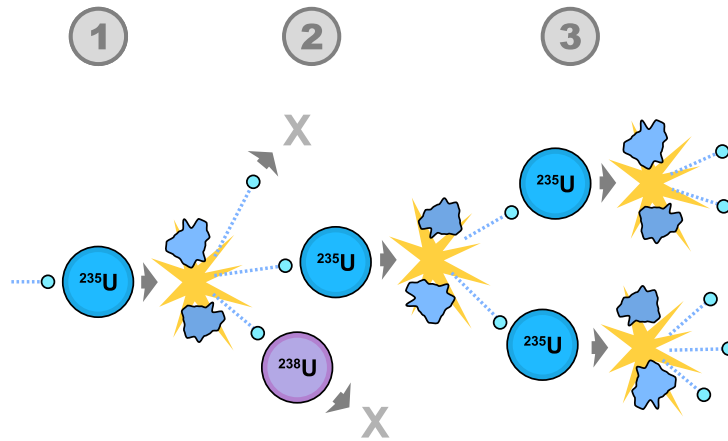


Figure 2.3: The figure illustrates a fission chain reaction. [32]

Current nuclear fission reactors are designed around the fission chain reaction. They can be used for a range of different purposes, e.g. radioisotope production, neutron-based research or power generation. The focus of this thesis is on power reactors where the goal is to use convert the energy released during fission to electricity. Typically this is by using the heat produced by fission reactions to generate steam to run turbines, which are connected to generators that produce electricity. [16]

2.2.1 Neutron Transport

The fission rate and the fission rate distribution and therefore power of a nuclear reactor is largely determined by the distribution of neutrons. To understand the behaviour of a reactor it is therefore crucial to accurately model the movement and distribution of neutrons. This problem is called the neutron transport problem.

For a mathematical description of the neutron transport problem it is useful to define two quantities, the angular neutron density $\tilde{n}(\mathbf{r}, \hat{\Omega}, E, t)$ and the angular neutron flux $\psi(\mathbf{r}, \hat{\Omega}, E, t)$. These describe the neutron density, and rate of neutron streaming in 6-dimensional phase-space, with \mathbf{r} being a

position, $\hat{\Omega}$ being a direction of motion and E being the kinetic energy of the neutrons. [16] They are related by:

$$\psi(\mathbf{r}, \hat{\Omega}, E, t) = v\tilde{n}(\mathbf{r}, \hat{\Omega}, E, t) \quad (2.4)$$

Where, v is the neutron velocity.[16]

These two quantities are not directly measurable, however they are closely related to the more physical neutron density n :

$$n(\mathbf{r}, E) = \int_{4\pi} \tilde{n}(\mathbf{r}, \hat{\Omega}, E) \quad (2.5)$$

and scalar flux density $\phi(\mathbf{r}, E)$:

$$\phi(\mathbf{r}, E) = \int_{4\pi} \psi(\mathbf{r}, \hat{\Omega}, E, t) \quad (2.6)$$

and reaction rates can be related to them via:

$$R = \int_0^\infty \int_{4\pi} \int_V d^3r d\hat{\Omega} dE n(\mathbf{r})\sigma(E)\psi(\mathbf{r}, \hat{\Omega}, E) \quad (2.7)$$

The neutron transport problem is typically described using the neutron transport equation:

$$\frac{1}{v} \frac{\partial}{\partial t} \psi + \hat{\Omega} \cdot \nabla \psi + \Sigma_t(\mathbf{r}, E)\psi = q(\mathbf{r}, \hat{\Omega}, E, t) \quad (2.8)$$

this equation is derived from the Boltzmann equation.¹ [16, 6] The terms on the left hand side of the equation correspond to (from left to right):

1. The rate of change w.r.t. time of the angular neutron density.
2. The rate at which neutrons moving along direction $\hat{\Omega}$ enter and leave the volume element d^3r .
3. The interactions removing neutrons either by scattering or absorption.

The term on the right hand side is the source term $q(\mathbf{r}, \hat{\Omega}, E, t)$, it describes the rate at which neutrons enter the phase-space element. Traditionally this term is broken into three different parts: external neutrons, neutrons produced through fission and neutrons entering the phase space element $d^3r d\hat{\Omega} dE$ through scattering. [16, 6] Let us denote these as:

$$q(\mathbf{r}, \hat{\Omega}, E, t) = q_{\text{ext.}}(\mathbf{r}, \hat{\Omega}, E, t) + q_f(\mathbf{r}, \hat{\Omega}, E, t) + q_s(\mathbf{r}, \hat{\Omega}, E, t) \quad (2.9)$$

¹Some literature may call this equation the Boltzmann equation. It should be noted however that the transport equation as stated here is actually a linearised form of the more general Boltzmann equation.

The external source term will be ignored from here, as it is not relevant for typical reactor operation. It describes neutrons introduced into a system from an external neutron source.

The scattering term, q_s , describes the contribution of scattering. Mathematically the scattering term is described as:

$$q_s(\mathbf{r}, \hat{\Omega}, E, t) = \int_{4\pi} \int_0^\infty dE' d\hat{\Omega}' \Sigma_s(\mathbf{r}, \hat{\Omega}' \rightarrow \hat{\Omega}, E' \rightarrow E) \psi(\mathbf{r}, \hat{\Omega}', E', t) \quad (2.10)$$

where $\Sigma_s(\mathbf{r}, \hat{\Omega}' \rightarrow \hat{\Omega}, E' \rightarrow E)$ is the macroscopic cross-section for scattering from direction $\hat{\Omega}'$ to $\hat{\Omega}$ and energy E' to E . [16, 6] Note that this equation technically should be a sum over the macroscopic cross-section for individual nuclei, to simplify notation this was omitted here.

The fission term, q_f , can be described somewhat similarly. The production rate for fission neutrons in the phase space element will depend on the energy spectrum of the fission neutrons $\chi(E)$,² the average number of neutrons produced per fission reaction ν ,³ and the fission rate. Mathematically the fission source term can be described as:

$$\begin{aligned} q_f(\mathbf{r}, \hat{\Omega}, E, t) &= \chi(E) \int_{4\pi} \int_0^\infty dE' d\hat{\Omega}' \nu \Sigma_f(\mathbf{r}, E') \psi(\mathbf{r}, \hat{\Omega}', E', t) \\ &= \frac{\chi(E)}{4\pi} \int_0^\infty dE' \nu \Sigma_f(\mathbf{r}, E') \phi(\mathbf{r}, E', t) \end{aligned} \quad (2.11)$$

where $\nu \Sigma_f$ is the fission neutron production factor (treated as a single quantity). Fission neutrons are emitted isotropically, it is therefore possible to integrate the angular flux density to obtain the scalar neutron flux $\phi(\mathbf{r}, E, t)$. This equation should technically also be a sum over all nuclei that can undergo fission. [16, 6]

2.2.2 Criticality

A reactor is said to be super- or sub-critical if the power is increasing or decreasing, respectively. Normally the aim is to keep the power constant in a nuclear reactor, i.e. to keep the flux constant. A reactor operating at constant power is said to be critical, the neutron flux is in equilibrium. [16]

At equilibrium the angular neutron density and flux has no time dependence. The transport equation (eq. (2.8)) at equilibrium therefore becomes:

$$\hat{\Omega} \cdot \nabla \psi(\mathbf{r}, \hat{\Omega}, E) + \Sigma_t(\mathbf{r}, E) \psi = q(\mathbf{r}, \hat{\Omega}, E) \quad (2.12)$$

This equation is sometimes referred to as the equilibrium equation. Its solution describes a critical system, where the number of neutrons produced is equal to the number of neutrons lost.[16]

²Both the energy spectrum and the number of fission neutrons have a dependency on the incident neutron energy, however it is constant at neutron energies observed in nuclear reactors.[11]

³See footnote 2

By introducing the eigenvalue $1/k_{\text{eff}}$ on the fission source term the criticality problem can be formulated as an eigenvalue problem:

$$\hat{\Omega} \cdot \nabla \psi(\mathbf{r}, \hat{\Omega}, E) + \Sigma_t(\mathbf{r}, E)\psi = q_{\text{scatter}}(\mathbf{r}, \hat{\Omega}, E) + \frac{1}{k_{\text{eff}}} q_{\text{fission}}(\mathbf{r}, \hat{\Omega}, E) \quad (2.13)$$

The eigenfunction obtained from solving this eigenvalue problem, sometimes called the eigenflux, describes the shape of the angular neutron flux distribution. [6] It does not however describe the absolute flux, because the system is artificially forced into a steady state even if it is super- or sub-critical. To obtain a physically correct flux the solution would need to be normalised and rescaled to the physical system, based on e.g. the fission power.

The eigenvalue, or effective multiplication factor, k_{eff} , directly relates to the states described at the start of this section. A critical system has $k_{\text{eff}} = 1$, with $k_{\text{eff}} < 1$ and $k_{\text{eff}} > 1$ corresponding to sub- and super-critical respectively.[16]

A term sometimes used when discussing criticality, especially when comparing the impact of changes to reactor systems is the reactivity ρ , typically measured in pcm (per-cent-mille, 10^{-5}). This is defined through k_{eff} as:

$$\rho = \frac{k_{\text{eff}} - 1}{k_{\text{eff}}} \quad (2.14)$$

2.2.3 Solving the Transport Problem

There are a number of different approaches to solving the neutron transport problem ranging from fully analytical to deterministic and stochastic numerical approaches. Strictly analytical approaches are only feasible for highly theoretical problems and are rarely directly applicable to practical problems or reactors. This is due to the complex nature of the transport equation, as can be seen from equation (2.8) it depends on both the derivative and integral of the angular neutron flux, a characteristic that remains in the steady-state case seen in equation (2.13).

The details of analytical or deterministic approaches will be left out here as it is a very broad topic with many different approaches. The interested reader can find more details in any number of reactor physics textbooks, e.g. Duderstadt. [6] Briefly, deterministic approaches for realistic problems rely upon approximations, e.g. to reformulate the transport equation into a more manageable PDE. This makes them (generally) cheap computationally, and very useful for e.g. optimisation problems that require iterative variations in the geometry. However, due to the approximations involved deterministic solvers often come with an increased setup cost compared to stochastic approaches.

For the work presented here it was determined that this additional setup cost outweighed the savings in computational time and a Monte-Carlo based, i.e. stochastic, solver was used instead. Monte-Carlo based solutions to

the transport simulate the motion and interactions of individual neutrons through the reactor. This involves very few approximations, and enables very high accuracy if enough neutrons are simulated. However, it comes at the cost of computational time as simulating the motion of a large number of neutrons individually is costly.

Monte-Carlo neutron transport codes typically simulate neutrons in generations, sometimes called batches. Each generation begins by sampling neutrons from the previous generation. During the simulation captured neutrons are removed from the list of active neutrons, those that scatter are kept and fission events add new neutrons to the list. [16]

The simulation is typically initiated by a random neutron distribution (or perhaps an “educated guess”), which over successive generations converge towards the true distribution of the simulated geometry. It is important to ensure this convergence has occurred before measuring e.g. reaction rates, as this is only meaningful with the true distribution. A common metric for this is the Shannon entropy, a measure of the disorder of the fission source distribution. When the fission source distribution has converged the Shannon entropy will reach equilibrium. The Shannon entropy is defined as follows for a random variable X :

$$H(X) = \sum_{i=1}^n p_i \ln p_i \quad (2.15)$$

where p_i is the probability for a neutron from the active list to be e.g. in a specific region of the geometry (depending on which random variable is studied). [20]

Reaction rates, fluxes, and many other quantities can be obtained from Monte-Carlo simulations by simple tallying of neutron interactions. Typically these need to be defined before a simulation is started. Due to the large number of interactions occurring during a simulation it is not feasible to store every interaction. Typically these tallies are recorded separately each generation. This makes it possible to compute both the mean, and the uncertainty as the standard deviation. [16]

2.2.4 Burnup & Depletion

Previous sections have considered the materials in a reactor as static, and unchanging with time. This is a simplification, in reality fission consumes fissioning nuclei and the production of fission products, capture reactions transmute one nucleus into another, and unstable nuclei undergo radioactive decay. Over longer time scales this leads to significant changes in the isotopic composition of the core, which will impact the macroscopic cross-sections seen in eq. (2.8) and thus impact the neutron population. This is the burnup

problem, typically modelled using the Bateman equations:

$$\frac{d\mathbf{N}(\mathbf{r}, t)}{dt} = \mathbb{M}(\phi, T)\mathbf{N}(\mathbf{r}, t), \quad (2.16)$$

where \mathbf{N} is the nuclide field describing the distribution of every nuclide species throughout space as a function of time. The matrix \mathbb{M} is the transmutation matrix, containing coefficients describing the rate of change of every nuclide into every other. [20]

The transmutation matrix contains two main contributions, a constant matrix of decay constants \mathbb{D} and a contribution from neutron-induced reactions. The latter is computed by integrating the product of the scalar flux and the cross-section over energy. [20] In equation form this can be written as:

$$\mathbb{M}(\phi, T) = \int_0^\infty \phi(\mathbf{r}, E, t)\mathbb{X}(T) dE + \mathbb{D}, \quad (2.17)$$

Assuming constant flux the analytical solution to the Bateman equations can be written as:

$$\mathbf{N}(t) = \mathbf{N}_0 \exp(\mathbb{M}(\phi, T)(t - t_0)) \quad (2.18)$$

In general of course, the flux will be time-dependent because of the changing isotopic composition. [20]

2.2.5 Solving The Burnup Problem

Solving the Bateman equations is generally very challenging owing to the dependence of the transmutation matrix on the flux, which in turn depends on the nuclide field. For this reason numerical approaches are generally required. Typically numerical ODE solvers are used in conjunction with neutron transport codes. This is a very computationally costly problem because of the need to compute the flux every time-step. [20]

Step-by step a numerical solution to the Bateman equations might look something like:

1. Compute reaction rates (e.g. using Monte-Carlo transport, or via flux)
2. Lookup decay constants for nuclide field
3. Assemble transmutation matrix \mathbb{M}
4. Perform step using ODE solver
5. Repeat steps 1-4 until desired time is reached

As can be seen from step 1 above, this involves repeatedly solving for reaction rates. This becomes computationally expensive very quickly, and it is not uncommon for calculations to take many weeks.

The Bateman equations are simplified slightly compared to equation (2.16) when performing numerical calculations by dividing the geometry into depletion zones. With each zone having its own nuclide inventory, instead of solving for a continuous nuclide field $N(\mathbf{r}, t)$. This is done to reduce the memory footprint and processing time as a very large number of nuclides need to be considered in a nuclear reactor. [20]

2.2.6 Core Loading & Fuel Management

The evolution of the isotopic composition of the fuel during operation creates significant operational challenges. Depletion causes changes in reactivity depending on burnup, and because the power distribution in a reactor is never quite flat, this will cause local power peaking. The difficulty in managing peaking during burnup has led to the general consensus that the ideal power distribution of a reactor core is flat. [29]

To obtain a flat power distribution the loading is used, i.e. how the fuel is installed in the reactor. This is done in two main ways: varying local enrichment and multi-batch loading. The reactivity is naturally lower for fuel with a lower enrichment. Strategic variation of the enrichment in the core can therefore counteract the effects of variations in burnup. [29]

Multi-batch loading is conceptually similar, however, it instead involves the mixing old and new fuel in the reactor core. A reactor is typically only refuelled once every 12 to 18 months, this period is called a cycle. For multi-batch loading, only a fraction of the fuel in the reactor is replaced at the end of every cycle, and the partially burned fuel in the reactor is strategically reshuffled to create as flat a distribution as possible. [29]

For more precise local power control, control rods and burnable absorbers may also be used. However, the use of control rods and locally applied burnable absorbers has to be somewhat limited as it can also lead to power peaking. Depending on the absorber used the local flux suppression can be very strong. [29] Burnable absorbers will be described in more detail later (see section 2.5).

Optimising a core design is a very difficult problem, often involving iterative burnup calculations of the entire core. Fuel placement, burnable absorber application and control rod insertion all needs to be optimised to create a core which lasts the desired cycle length. Core design engineers want as many options as possible to tweak the power distribution for the core design problem to be tractable.

2.3 Types of Nuclear Reactors

A broad range of different designs exists for nuclear reactors that utilise different geometries, means of moderation and fuel. The focus of this thesis is mainly on light water reactors, and more specifically pressurized water

reactors (PWRs) as that is where IFBA has been applied historically. For the purposes of the discussion, however, boiling water reactors (BWRs) will also be presented here.

Light water reactors (LWRs) are a class of reactors which utilize thermal neutrons through moderation with light (normal) water. The neutron energies in these reactor systems are typically below 0.1 eV. In addition to acting as a moderator, the light water also acts as a coolant in LWRs, ensuring that the fuel stays safely within thermal limits. [29]

The key difference between the two types of LWRs is that a PWR uses high pressures to maintain a single phase in the coolant, typically on the order of 15.5 MPa. A BWR operates at lower pressures, typically around 7.2 MPa, allowing the coolant to boil inside the reactor vessel and creating a two-phase steam-water mixture. [29] The following sections will describe the basic structure of each of these two reactor types.

2.3.1 Pressurised Water Reactors

The pressurised water reactor was originally developed by the United States during the late 1940s, but they have since been constructed in many other countries. It is the most common nuclear power reactor type. The basic concept behind a PWR is relatively simple: the core is an array of fuel assemblies, where each assembly is itself an array of fuel rods, alongside control rods, burnable poisons and instrumentation. The entire core is submerged in water at high enough pressure to prevent it from boiling. [29]

The fuel rods are typically around 1 cm in diameter, with UO_2 fuel at 2 - 4 % enrichment. Sometimes burnable absorbers are added, either by mixing in Gd_2O_3 , or an IFBA coating of ZrB_2 . The fuel itself will be discussed in more detail in section 2.4, and burnable absorbers will be described in section 2.5. The rods are clad in a coating of Zircaloy-4 or a similar Zirconium based alloy. [29, 15]

Reactivity control is typically discussed in terms of long- and short-term reactivity control, based on the timescale for the desired reactivity change. Long term reactivity control, i.e. control on the time-scale of an entire fuel-cycle, is in PWRs achieved through the management of boric acid concentration. The coolant in a PWR contains boric acid, this reduces reactivity because boron is a strong neutron absorber. However, there is a limit to how much boric acid can be added to the core, because the boric acid introduces a positive moderator temperature coefficient which can become a safety risk. This is due to the reduction of the absorption cross-section with temperature. [29] Boric acid also carries with it limitations due to material corrosion and degradation due to its low pH. These types of effects are firmly outside the scope of this thesis, but it is nevertheless important to note that core design is often constrained by chemical or material considerations. [19]

The safety implications of high boric acid concentrations make it de-

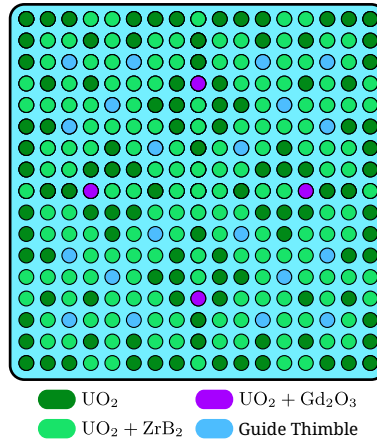


Figure 2.4: Top-down view of PWR fuel assembly containing standard UO_2 fuel rods alongside IBA, IFBA and open positions for instrumentation/control rods (guide thimbles).

sirable to have additional means of long-term reactivity control. One such method is burnable absorbers in various forms. For PWRs, many different forms of burnable absorbers are used, often in combination, such as burnable absorber rods, IBA rods, and IFBA rods. [29] IBA and IFBA will be described in more detail in section 2.5.

Short-term reactivity control is performed using control rods. There are two types of control rods in a PWR: regulating rods and scram rods. Regulating rods can be partially extracted and inserted to give quick fine-grained control over reactivity. Crucially, they are much faster than adjusting the boric acid concentration. The second type, scram rods, are designed to be held outside the core and inserted to rapidly decrease reactivity and shut down the core. [29]

2.3.2 Boiling Water Reactors

The fundamental difference between boiling water reactors and PWRs is that the water inside a BWR is allowed to boil. The core thus contains a two-phase water-steam mixture. This is key because water is a better moderator than steam, this is due to water's higher density which leads to a higher macroscopic cross-section. This produces what is called a negative temperature coefficient. The reactivity of the core decreases with temperature because a higher temperature produces more steam, which reduces moderation.

Structurally, the boiling water reactor is in many ways similar to the PWR. Similar to the PWR core, the BWR core contains fuel assemblies, made up of fuel rods. However, BWR fuel assemblies are smaller than PWR assemblies, with some variation depending on the design. Historically

BWRs have used 10×10 assemblies which may look something like figure 2.5 with a cross-shaped void in the middle for a control-rod. Newer designs are moving towards 11×11 assemblies with a complex combination of part-length rods and water rods to improve efficiency and fuel economy. The individual rods in BWR fuel are typically slightly larger than the rods in a PWR, with a diameter of ~ 1.3 cm. [29]

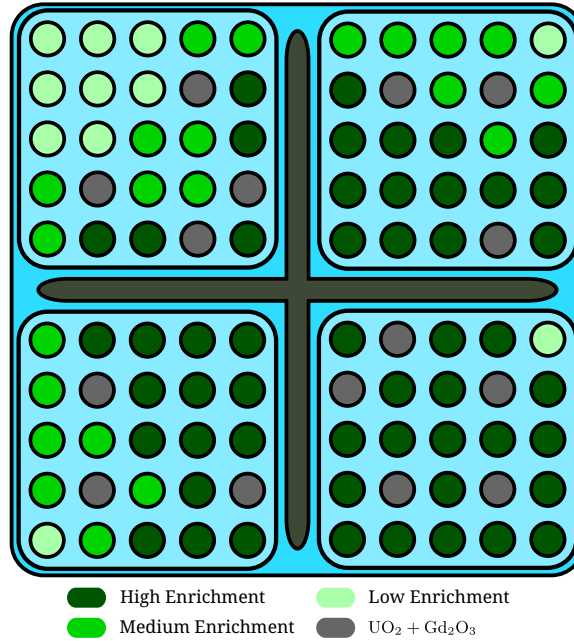


Figure 2.5: An example of a BWR fuel module, showing a 2×2 grid of fuel assemblies around a control rod. Note that the fuel distribution is only illustrative, real distributions vary based on the core design utilised.

To compensate for the long-term reactivity drop caused by fuel depletion two mechanisms are used. The first is the cross-shaped control rods which are slowly extracted, increasing reactivity. The second is burnable absorbers, specifically gadolinia (Gd_2O_3). This burnable absorber introduces a reactivity penalty early in the cycle, which drops while the fuel is being consumed. [29]

Shorter-term reactivity control is handled by adjusting the coolant flow rate and the control rods. A higher coolant flow rate decreases coolant temperature, and therefore boiling. This improves moderation, increasing reactivity. Conversely, the reactivity can be decreased by reducing the coolant flow rate allowing more boiling. [29]

2.4 LWR Fuel

The fuel rods used in LWRs are typically filled with fuel in the form of ceramic pellets of UO_2 , or $(\text{U}, \text{Pu})\text{O}_2$ for MOX (mixed oxide) fuel. This is produced by pressing a powder into the shape of the pellets followed by sintering. Sintering is the process of heating the pellets under high pressure, creating a bond between the powder particles, and forming a solid pellet. [24]

On a microscopic level, the solid pellet consists of bonded grains, around $10 \mu\text{m}$ in size for normal fuel. Typically the fuel has a density $\sim 95 \%$ of the theoretically perfect density. This is due to imperfect sintering, which leaves microscopic voids in the structure open. These voids, sometimes called pores, are left by design as they give space for gaseous fission products. [24]

The following sections will start by giving a general overview of the evolution of the fuel behaviour and then describe to specific concepts in more detail, fuel fragmentation, relocation and dispersal (FFRD) and the high burnup structure (HBS). Both of these have a high potential to be affected by the addition of IFBA.

2.4.1 Evolution During Burnup

The radial and axial temperature distribution in the fuel is mainly a function of the linear power density, with a higher power density leading to a steeper temperature gradient and higher centreline temperature. However, other factors contribute as well, such as the geometry of the pellet, especially the gap between the fuel and cladding, the fuel-cladding interaction, and the burnup. During burnup, the thermal conductivity of the fuel degrades due to the accumulation of fission products and radiation-induced defects in the fuel matrix. [24]

During the first stage of irradiation the fuel will also experience a phenomenon known as densification, or irradiation sintering. Densification will cause the pellets to shrink initially, however, as irradiation continues fission gases will begin to build up in the fuel. These will cause swelling which eventually wins over densification, causing the fuel to grow in volume. [24] At around 30 MWd/kgU swelling causes the gap between the fuel and cladding to close.

Initially, the fuel-cladding interaction after the gap has closed is purely mechanical, mainly contact pressure and friction. At this stage, if irradiation is stopped and the fuel is allowed to cool, the fuel will detach from the cladding. However, if irradiation continues a strong chemical bond will be created between the fuel and the cladding, which keeps the gap closed even after irradiation has stopped. [24] The chemical bond takes the form of a transition region where it is not possible to determine where the fuel ends and the cladding begins. It is characterised by significant inter-diffusion of

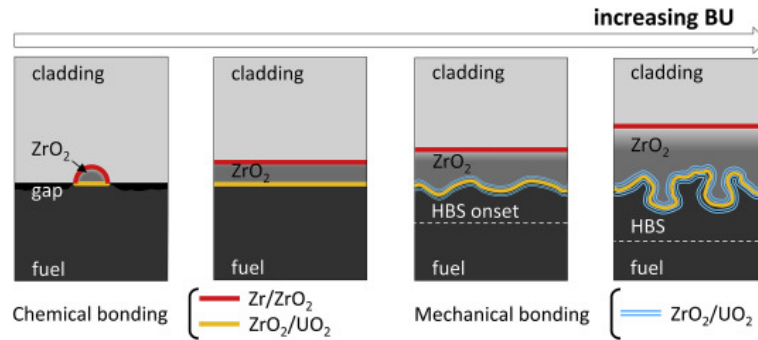


Figure 2.6: The figure shows the evolution of the fuel-clad bond with increasing burnup. Figure included with licence from copyright holder. [4]

fuel and zirconium, and the presence of zirconia. The process is illustrated in figure 2.6. [4]

2.4.2 High Burnup Structure

During irradiation the fuel will accumulate radiation damage, mainly from high energy fission products dislocating atoms from the fuel matrix. At the rim of a pellet at high burnup this accumulation of damage causes a restructuring of the fuel into what is known as the high burnup structure (HBS). The HBS is characterised by significantly smaller grains in the fuel, moving from $\sim 10 \mu\text{m}$ to sub-micrometre grains. [24, 18]

This formation starts at the rim of a pellet because that is where the local burnup is highest, typically around 60 MWd/kgU local burnup. The local burnup is the highest towards the rim because the rim experiences the highest thermal flux. The thermal flux is higher closer to the moderator since that is where neutrons are slowed to thermal energies. Additionally, the temperatures are much lower at the rim than at the centre, this is important because the high temperatures experienced at the centre of the fuel will anneal the accumulated radiation damage. Because of this the HBS requires temperatures below $\sim 1200 \text{ }^\circ\text{C}$ to form. [18]

The impact of the restructuring into HBS is complex and not fully understood, it is an active area of research. [26, 33] However, it has been observed that the HBS is a significant contributor to fission gas release at high burnup, approaching 100 MWd/kgU. [26] It has also been observed that the HBS can cause significant fission gas release during high temperature transients which can occur during e.g. loss of coolant accidents (LOCA) or reactivity initiated accidents (RIA). [23] These significant releases during transients can endanger the integrity of the cladding.

2.4.3 Fuel Fragmentation, Relocation and Dispersal

As was mentioned above thermal stresses in the fuel lead to the formation of microscopic cracks. On the macroscopic scale thermal stresses eventually lead to the formation of cracks in the fuel pellets. [24] This occurs under normal operation but especially during transients, i.e. short-lived deviations from stability in power, flux, temperature or pressure.

The presence of cracks in the fuel is in and of itself not necessarily a safety concern, despite cracks the fuel can maintain its structural integrity so long as the cladding remains intact. However, fuel fragmentation, especially fine fragmentation, has been determined to increase the risk of relocation, i.e. the collapse of the fuel stack inside the rod which in turn can cause additional strain on the cladding increasing the risk of coolant channel blockages or cladding ruptures. It also increases the risks associated with ruptures as fine fragmentation increases likelihood, and amount of dispersal. [24]

The main contributing factor to fuel fragmentation appears to be burnup. The characteristics of the fragmented fuel are however quite sensitive to other properties, for instance high burnup structure seems to lead to smaller fragments. [24] FFRD introduces risks that significantly hamper safety margins at high burnup, new strategies for managing it is critical for increasing fuel utilization. The local effect from a burnable absorber coating the fuel (such as IFBA), suppressing fission at the rim, could potentially enable this.

2.5 Burnable Absorbers

Burnable absorbers (BA) are made of nuclei with high neutron capture cross-sections, sometimes called neutron poisons. They can be used for a number of different purposes such as: long term reactivity control to allow for extended fuel cycles, optimisation of the power distribution in the core, or reducing wear on control rods. [7] Burnable absorbers are implemented in many different ways depending on the specific reactor and core loading strategy. Examples of implementations range from full rods of BA, simple plates inserted between assemblies, rods with fuel-BA mixtures and rods with fuel coated in BA. [7]

The core idea behind a burnable absorber is that the burnable absorber will capture neutrons, thus stopping them from contributing to the chain reaction. Thus suppressing reactivity. However, because there is a limited amount of the burnable absorber in the core, it will eventually deplete, making the effect temporary. The rate of neutron capture, and burnout rate of the absorber, will be determined by the cross-section of the burnable absorber and the flux through it. The reaction rate in the burnable absorber

is described by:

$$R = N_{\text{ba}} \int \sigma_{\text{ba}}(E) \Phi(E) \, dE \quad (2.19)$$

where N_{ba} describes the number of BA nuclei, $\sigma_{\text{ba}}(E)$ is the cross-section as a function of neutron energy and $\Phi(E)$ is the flux through the absorber as a function of energy. [29]

Note the energy dependence of the absorption cross-section here. Typically absorbers are categorised as either $1/v$ or resonance absorbers, based on the dominating behaviour in the absorption spectrum. The former, $1/v$ absorbers, predominantly capture neutrons in the thermal region, where the absorption cross-section is proportional to the inverse of the neutron velocity. For instance boron-10, gadolinium-155 and 157 are $1/v$ absorbers. Resonance absorbers instead mainly capture neutrons through peaks in the resonance region at intermediate neutron energies through resonance peaks. Figure 2.7 shows the absorption spectrum a $1/v$ absorber (^{10}B) alongside a resonance absorber (^{167}Er). [7]

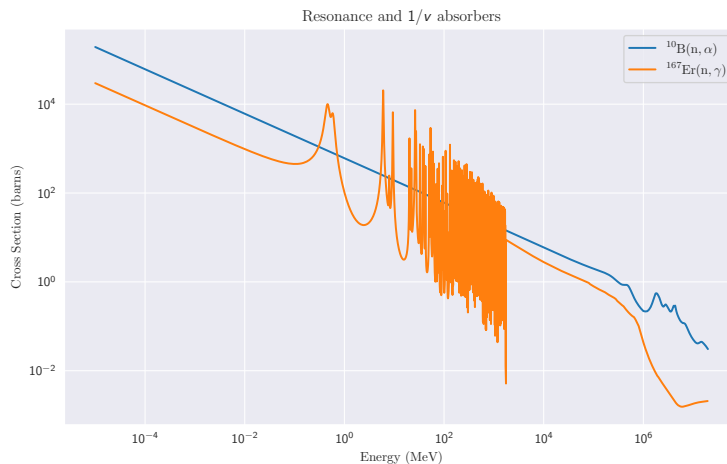


Figure 2.7: The figure shows the energy dependence of the cross-section for the most common absorption reactions for boron-10, a $1/v$ absorber, and erbium-167, a resonance absorber.

The different absorption spectrum has effects beyond different reaction rates depending on the neutron spectrum of the reactor. Due to how cross-sections are affected by temperatures $1/v$ absorbers tends to have a net positive reactivity feedback with increasing temperature. This is due to the capture cross-section decreasing with temperature. Resonance absorbers have the opposite effect due to Doppler broadening, which increases the width of the resonance peaks increasing the probability a neutron matching the peak energy. Ideally, a burnable absorber would have a negative

temperature feedback as it helps reduce the risk of a reactivity induced accident. However, in reality the negative temperature feedback of the fuel often overpowers any positive feedback effect from the burnable absorber so it is rarely a major consideration.

2.5.1 Integral Burnable Absorbers

Gadolinia, or Gd_2O_3 , has historically been used as a burnable absorber by mixing UO_2 with Gd_2O_3 into a homogeneous mixture. Rods with this type of homogeneous fuel-BA mixture are sometimes referred to as integral fuel burnable absorber (IBA) rods. This type of fuel has been successfully used since the 1960s. [10] A typical application of gadolinia sees a reactor loaded with a mixture of regular UO_2 rods alongside gadolinia rods. The gadolinia loading per rod, the ratio of gadolinia to UO_2 rods, and the placement of the gadolinia rods enables very granular planning of fuel burnup and reactivity. [15]

Gadolinia does have an impact on the material properties of the fuel, but not a large impact based on post irradiation examination of gadolinia rods. With regards to thermal properties it has been determined that thermal expansion, the specific heat and the melting-point all are largely unchanged compared to regular UO_2 fuel at the concentrations used in current fuel designs. Only the thermal conductivity requires some consideration, it is slightly lower in gadolinia fuel due to additional point defects. [10]

Reduced thermal conductivity leads to slightly increased temperatures in the fuel, a slightly higher rate of fission gas release and slightly higher pressure in the fuel rod. Experimental testing has however shown this effect to be minor at low gadolinia concentrations. Similarly, the mechanical properties of gadolinia rods have been observed to be similar to non-gadolinia rods, with no major adverse effects from the BA additive. [10]

2.5.2 Integral Fuel Burnable Absorbers

An alternative to IBA developed by Westinghouse is IFBA. The idea behind IFBA is that instead of adding the absorber into the fuel material the BA is added as a coating. [28] This has a number of benefits, with the main benefit being that the actual fuel pellet is the same as in normal fuel. An illustration of an IFBA rod is shown in figure 2.8, with the fuel pellet in green, the IFBA coating in yellow and the cladding in grey.

In the United States IFBA rods have seen widespread use in production. In total, as of 2018, over 4 million IFBA rods have been used across more than 40 nuclear plants, with production reaching approximately 250,000 rods per year. [31] Despite this there has curiously been very limited post irradiation examination of IFBA rods, as such the effects on the fuel are not fully known but are presumed to be negligible.

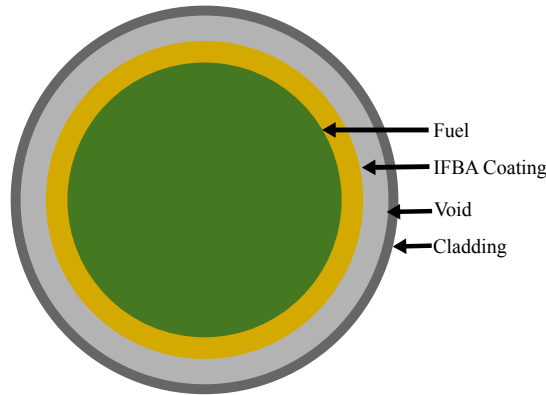


Figure 2.8: Cross-section of an IFBA rod. Fuel shown in green, IFBA coating in yellow, cladding in grey.

Westinghouse uses the material zirconium diboride (ZrB_2) for its IFBA rods. There are many benefits to ZrB_2 , but also a few drawbacks. It is easy to apply using vapour deposition and has a very high thermal conductivity, higher than UO_2 , and will therefore not harm thermal transfer from the fuel. However, the main capture reaction in ZrB_2 is the $^{10}\text{B}(n, \alpha)$ reaction which produces lithium-7, see equation (1.1). [7] The lithium produced is thought to remain in the coating. However, the helium is not, it is released from the coating and contributes to increasing the rod internal pressure. [21, 28]

2.6 Overview of Candidate Coatings

The candidate coatings which have been considered in this work, along with some of their key properties are listed in table 2.1. Besides CdO and ZrB_2 , none of the specific compounds studied have seen any use as burnable absorbers, and with CdO mainly explored for specialised research reactors in the 1980s. [5] However, the elements combined with boron in many of the other borides have seen some use in other types of burnable absorbers.

Most of the elements that have been tried as burnable absorbers have done so in the form of fuel-BA solutions, akin to gadolinium IBA. The elements that have been used in this way include: gadolinium, erbium, dysprosium and europium. Only gadolinium and erbium sees any notable commercial use however, with gadolinium generally favoured due to cost. For use in fuel-BA mixtures dysprosium and europium seems to be explored, but seen little to no use. [7]

A number of elements are or have historically been used in control rods as well, namely dysprosium, europium, samarium, hafnium and erbium. Due to their high cross-sections they naturally fit for use as control rods. [7]

Table 2.1: The table shows the candidate coatings along with their molar mass (M), density (ρ), macroscopic cross-section (Σ), thickness (d) and the melting point (T_{melt}). Candidates marked * were simulated with 60% enriched ^{10}B .

Symbol	M (g/mol)	d (μm)	T_{melt} (K)	ρ (g/cm 3) ⁴	Σ (b/cm 3) ⁵
ZrB $_2$	112.85	15.00	3313	6.09	82.8
ZrB $_2^*$	112.04	15.00	3313	6.09	250.1
GdB $_6$	222.116	15.00	2783	5.311	1298.4
DyB $_6$	227.37	15.00	N/A ⁶	6.98	171.8
EuB $_6$	216.83	15.00	2473	4.96	208.9
SmB $_6$	215.22	15.00	2673	5.112	250.0
YbB $_6$	237.91	15.00	>2200 ⁷	5.61	109.3
HfB $_2^*$	199.31	15.00	3520	11.12	262.6
ErB $_4$	210.503	15.00	2633	7.00	107.3
CdO	128.413	15.00	1832	8.649	169.7

However, in lower quantities they may prove suitable as burnable absorbers.

The synthesis of most of the hexaborides appears fairly well documented, and while experience appears limited in the nuclear industry most have been extensively explored for use in other fields. [3] The notable exception being ytterbium hexaboride, there is exceedingly little published about it, but it seems to be synthesizable at least based on the neutron scattering experiment by Takahashi et al. in the 1990s. [30]

⁴Densities taken from the materials project. [12] Density assumed unchanged for compounds with enriched boron.

⁵Total absorption cross-sections computed using elemental values from NIST. [22]

⁶No reputable source provides a melting point, it is likely similar to the other hexaborides.

⁷Additionally described as stable at high temperatures by e.g. Zhou et al. [34]

Chapter 3

Methodology

Two different software tools will be utilized to study the behaviour of the different IFBA candidates. The first step will be to perform neutronics and burnup simulations using the neutron transport code Serpent 2. This will give insight into how the different coatings are consumed, how they affect the power distribution in the fuel over time and helium production in the IFBA coating.

Serpent does not model thermal or mechanical properties of the fuel rod. To obtain information about how the IFBA coatings affects these properties the Serpent results will be fed to the fuel performance code Transuranus. Specifically the power profile and helium production from Serpent will be used, Transuranus then models the thermal and mechanical properties of the rod. The connection between Serpent and Transuranus is illustrated in figure 3.1.

3.1 Neutronics

Neutronics calculations were performed using version 2.1.32 of the Serpent 2 Monte-Carlo based neutron transport code. The Joint Evaluated Fission and Fusion File (JEFF) version 3.3 was used for cross-section and decay data. The calculations were performed on a cluster operated by the division for applied nuclear physics at Uppsala University. Four nodes were used for running four different simulations in parallel, each node with 64 CPUs. ¹

The chosen geometry for the neutronics calculations was a 3×3 grid of PWR rods of infinite height, with reflective boundary conditions. With IBA/IFBA on the middle rod and the surrounding rods left without any burnable absorber this gives a realistic loading of 1/9. This is in line with typical loadings of IBA, but on the lower end for IFBA loadings. The typical number IFBA rods per assembly varies significantly depending on where in the core design and where in the core an assembly is placed, based on publicly

¹Each node had 4x 16 core AMD Opteron 6370P processors and 128 GB ram.

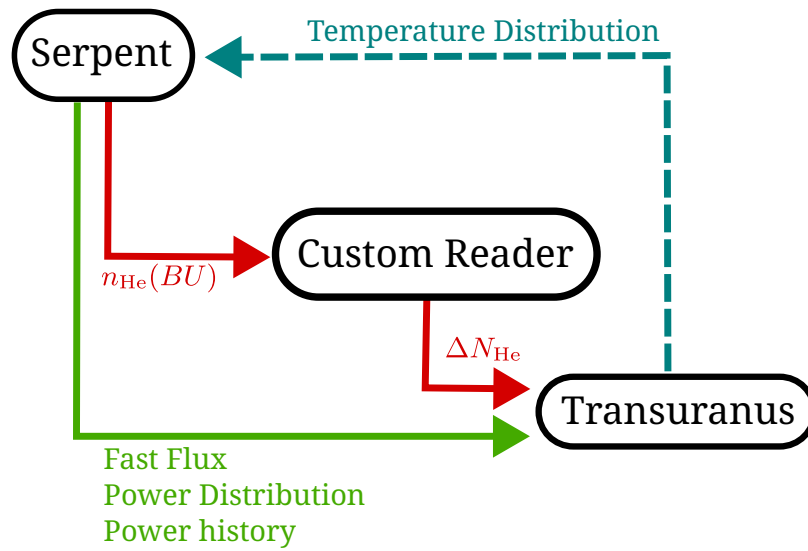


Figure 3.1: A diagram showing the properties extracted from Serpent for Transuranus. Also shown is a potential feedback of the temperature distribution from Transuranus to Serpent, this was not performed here but is a possible avenue for future research.

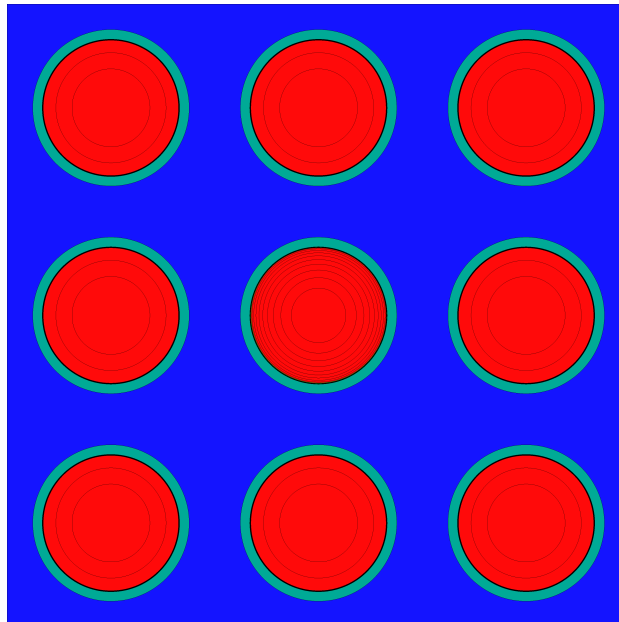


Figure 3.2: The geometry used for the neutronics calculations in Serpent.

available information it seems to range between 10%-50% for IFBA. [15] To control variables no other burnable absorber was included, e.g. no soluble boron was added in the coolant. An illustration of the geometry can be seen in figure 3.2.

The individual rods and the pitch of the grid was inspired by Westinghouse's AP1000 PWR as described by Laranjo De Stefani. [15] Table 3.1 shows a summary of the measurements of the fuel rods, along with the linear power.

Table 3.1: Specifications used to define the geometry, based on the AP1000 as described by Laranjo De Stefani. [15]

Measurement	Value	Unit
Fuel Radius	4.0975	mm
Gap Radius	4.1775	mm
Cladding Radius	4.7475	mm
Pitch	1.26	cm
Avg. Linear Power	192.0	W/cm rod

The simulated fuel was UO_2 with a 4.5 w/o U235 enrichment. This is a quite high initial enrichment for a PWR reactor, as would be used for longer fuel cycles where burnable absorbers are of interest. The cladding of the AP1000 is made of a proprietary alloy developed Westinghouse called Zircaloy, for the sake of simplicity Zircaloy-4 was substituted for this thesis. The neutronic effect of this change should be negligible, as both claddings are essentially transparent to neutrons.

Due to the temperature dependence of cross-sections temperatures need to be defined in Serpent, note however that these are temperatures are static in the simulation. The temperatures used here were again based on the AP1000 under normal operating conditions, the temperatures used are written in table 3.2.

Table 3.2: Assumed temperatures for the Serpent 2 calculations. Inspired by the temperatures in for the AP1000. [15]

Region	Temperature (K)
Fuel	900
IFBA coating	900
Cladding	610
Coolant	565

The same temperature was used for the entirety of the fuel and IFBA coating. In reality there will be a temperature gradient in the fuel rod. With higher temperatures towards the centre and the surface closer in temperature to the cladding. Neutron cross-sections decrease with temperature, therefore reaction rates observed towards the surface of the fuel will likely be somewhat lower than they should be because of this.

Similarly, the burn rate of the IFBA coatings observed here will be slightly reduced because of this, with slightly higher burn rates observed in reality. However, all candidates should be affected similarly and the different coatings should therefore remain comparable. It should be noted in case of future comparisons to the results shown here.

With regards to the IFBA coating, the choice was made to use the same thickness for all candidates. This was chosen as both the initial reactivity worth and burn rate varies between candidates. An argument could be made for comparing equivalent lifetimes or initial reactivity worths. For this work this was not done for two main reasons; there is not a lot of room to vary the thickness, realistically it is limited to 10-15 μm . Additionally, the computational cost of performing such an optimisation would be quite high, and computational time was already somewhat limited.

The specific choice of 15 μm was made as this is on the higher end of the feasible thickness and having an IFBA ratio of 1/9 is quite low. It is not uncommon for real core designs with IFBA loadings exceeding 50%.

In addition to the IFBA coatings, simulations were also made with standard UO_2 and IBA ($\text{UO}_2\text{-Gd}_2\text{O}_3$) middle rods without IFBA for the sake of comparison. A concentration of 3 w/o Gd_2O_3 was used for the IBA rod. The parameters described in the coming two sections are the same for these as for the IFBA candidates.

3.1.1 Criticality Calculation Parameters

Ideally parameters used for the criticality calculations would be set in terms of the relative error in the measured quantity with the highest uncertainty. However, due to limitations in the selectable output parameters in Serpent this is quite difficult to monitor and tune for. Instead the uncertainty target used was therefore 20 pcm relative error in k_{eff} up to 60 MWd/kgU. This relative error is in line with what is used for production simulations for core design. Testing showed that it produced sufficiently low uncertainty in all measured quantities.

Testing showed that the uncertainty in k_{eff} increased approximately linearly with burnup, figure 3.3 highlights this. Through trial and error it was found that 10000 neutrons per generation with 6000 active generations gave 20 pcm at 60 MWd/kgU. Furthermore, it was determined that for the small geometry used here convergence was not a concern. The fission source always converged within about 100 generations, which was therefore used for

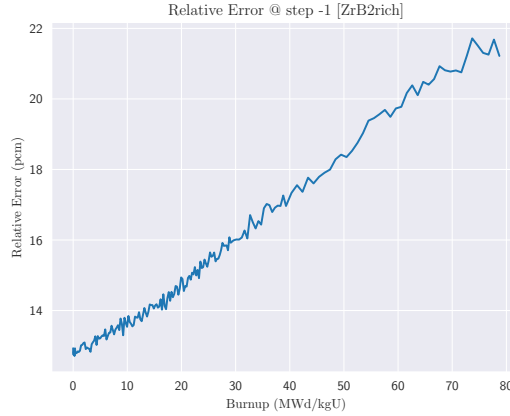


Figure 3.3: The figure shows the relative error in k_{eff} as a function of burnup for a run with the ZrB_2 rod.

the full simulations. Figures 3.4 and 3.5 show the Shannon entropy in each direction, as well as a convergence plot for k_{eff} .

With 6000 active generations, 100 inactive and 10000 neutrons per generation this resulted in a running time of about 40 minutes per cycle at the start of the burnup calculation, with about 70 minutes per cycle at 79 MWd/kgU.

3.1.2 Burnup Calculation Parameters

Serpent has built in functions for performing depletion calculations, i.e. solving the Bateman equations, eq. (2.16). This equation depends on both space and time via the nuclide field \mathbf{N} . Numerical treatment of the Bateman equation entails using a numerical ODE solver alongside particle transport for every time-step to estimate the transmutation matrix \mathbf{M} (see eq. (2.17)).

With regards to the temporal discretisation, it was decided to use a slowly increasing time-step size. This was done because time integration introduces accumulating discretisation errors, with smaller time-steps in the beginning having an outsized impact on the final result. Larger time-steps do however save a lot of computational time as a criticality calculation needs to be performed every time-step. In Serpent the step-size can be set in terms of burnup. It was decided to use a step-size of 0.1 MWd/kgU for the first 5 time-steps, followed by 0.25 up to 30 MWd/kgU, followed by 0.5 up to 36 MWd/kgU and finally 1.0 for the steps up to 79 MWd/kgU.

The recommended ODE solver in Serpent is the so-called predictor-corrector method. This is a solver that is specifically designed for stiff problems with high evaluation costs, making it very well suited to the Bateman equations. [14] It does however require two flux calculations for every time-

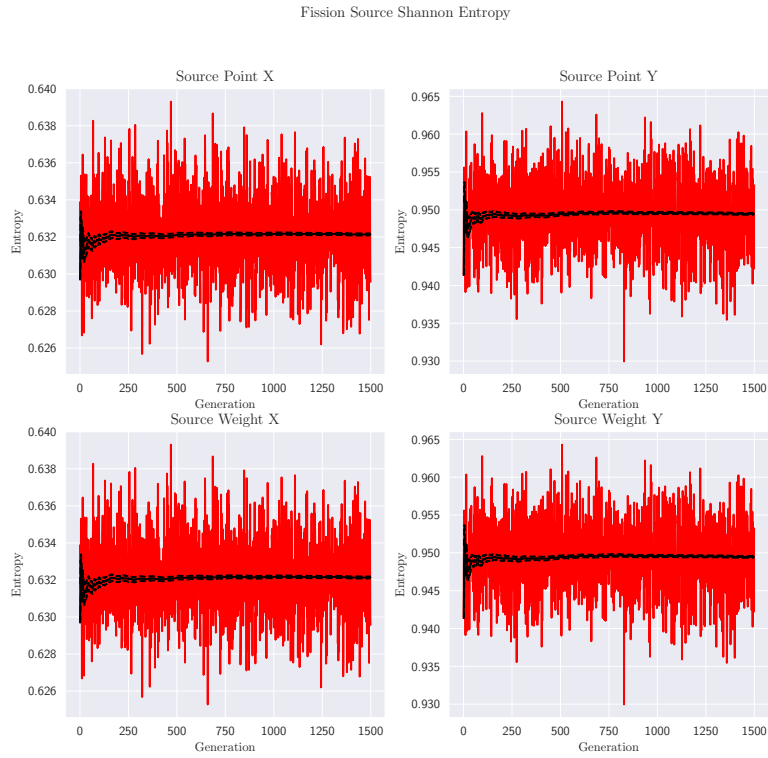


Figure 3.4: The figure shows the Shannon entropy for the fission source point and the fission source weight at the final time-step in the x and y directions.

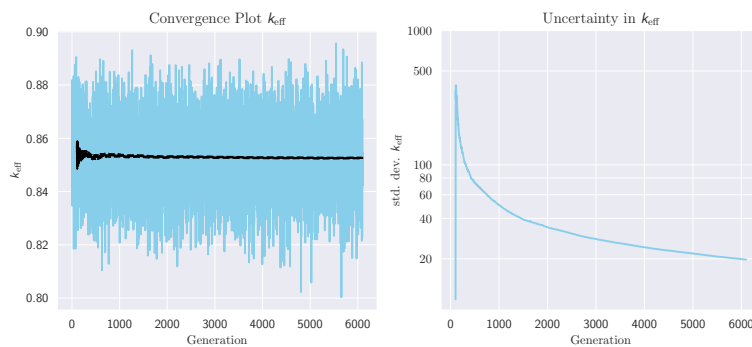


Figure 3.5: The left figure shows the value of k_{eff} as a function of generation, with the cumulative average as a solid black line, the uncertainty as a dashed line and the value for each generation as a solid blue line. The right figure shows the relative uncertainty of k_{eff} in pcm. Both figures are taken at about 60 MWd/kgU, with the ZrB_2 rod.

step, one for “prediction” and one for “correction”. The temporal discretisation used here results in 180 time-steps and thus 360 criticality calculations per burnup simulation. Using the parameters as described in section 3.1.1 for the criticality calculations this leads to a total runtime of just over 15 days per burnup simulation.

The spatial discretisation is used for the nuclide field in eq. (2.16), called depletion zones in Serpent. The inventory of the depletion zones are tracked for the burnup calculation. In figure 3.2 each of the fuel rod contains a number of rings, these are depletion zones. There are 3 depletion zones of equal volume for each of the non-BA rods. The middle rod has 10+1 zones, 10 in the fuel and one covering the burnable absorber coating.

Because the IFBA coating is expected to create a highly localized flux depression near the surface of the fuel the middle rod the size of the zones in the middle rod were skewed towards the rim to capture this. This was done using the following formula for the outer radius of zone n :

$$r_n = \frac{R}{\sum_{j=0}^N j^{0.77}} \sqrt{\sum_{i=0}^n i^{0.77}} \quad (3.1)$$

where R is the radius of the fuel pellet, N is the number of depletion zones and 0.77 is a constant determined to provide small zones towards the rim but large enough to still provide reasonable statistics. Figure 3.6 shows the area for depletion zones as a function of the radial position.

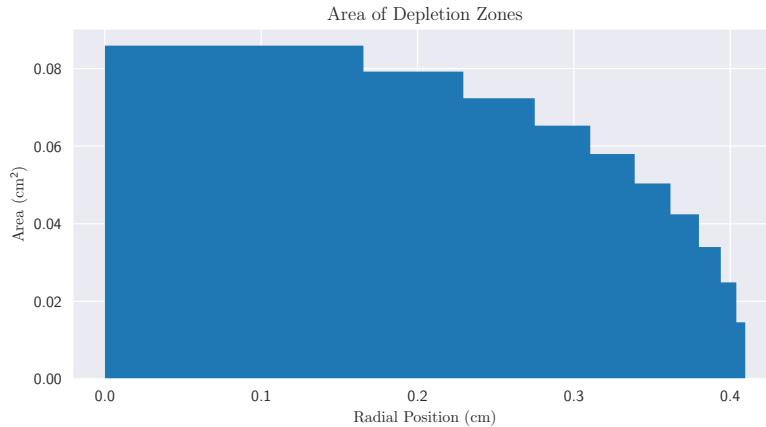


Figure 3.6: The figure shows the area of each depletion zone as a function of the radial position

3.1.3 Output Parameters & Post-Processing

Serpent by default tracks a number of useful quantities which are of interest for the current calculation such as k_{eff} and xenon-135 concentration. In addi-

tion to these, additional quantities can be tracked using so-called detectors. These can be used to measure a range of quantities such as reaction rates and neutron fluxes through a specific surface or in a volume. A number of these were added for the simulations performed here and can be seen in table 3.3, along with the reaction MTs which are used to define which reaction should be tallied in Serpent.

Table 3.3: The table shows the quantities tracked using detectors in Serpent, specifying the location they were measured, whether the quantity was tracked as a function of radius (subdivided) and the reaction MT used

Location	Subdiv.	MT	Quantity
Middle rod	Radial	-6	Fission rate
Middle rod	Radial	-8	Fission power
Middle rod	Radial	-2	Capture rate
Middle rod	Radial	18	U-235 fission rate
Middle rod	Radial	101	U-238 capture rate
IFBA coating	None	-57	Helium production
IFBA coating	None	-2	Total capture rate
Cladding, middle rod	None	N/A	Fast neutron flux

The results from Serpent were post-processed and analysed using the python library SerpentTools. [13] The post-processing applied here was relatively limited, only amounting to organizing the output data, unit conversions and interpolation to make direct comparisons easier.

Interpolation was used for individual output parameters as a function of rod average burnup. Rod average burnup will differ slightly between burnable absorbers because the burnable absorber will suppress the power of the rod it is applied to. Here, cubic interpolation was utilized to make radial comparisons or compute the difference at the same burnup.

3.2 Transuranus Setup

Transuranus is a fuel performance capable of modelling thermal, hydraulic and mechanical effects in a fuel rod during irradiation. In this work version v1m1j24 was used to model both normal and IFBA rods. Comparing the simulation results for normal and IFBA rods makes it possible to quantify the direct impact of the coating on the rods. The Transuranus simulation was based upon the neutronics calculations described above. In particular the linear heat rating, fast neutron flux, radial power distribution and

the helium production in the IFBA coating were taken from the neutronics results.

For the Transuranus simulations the the candidates with enriched boron had to be excluded due to excessive pressure build-up. The resulting pressures were over 20 MPa for the compounds with enriched boron. This is high enough that a real fuel rod would burst and therefore not worthy of more detailed fuel performance analysis. Additionally, due to time-constraints IBA rods were not modelled in Transuranus. Whilst Transuranus can model IBA rods, it would have required a significant amount of time to set up and the IFBA simulations were very time-consuming already.

3.2.1 Fuel Rod Characteristics

To accurately model the a fuel rod in Transuranus the properties of the fuel rod need to be provided. There is a very large number of configurable properties for this in Transuranus, this section will describe the key properties and especially highlight the ones that differ between an IFBA and regular rod. The basic idea was to model a relatively generic PWR rod, many parameters for this are provided by the Transuranus manual, however some deviations were made based on suggestions from the fuel performance department at Westinghouse. This section will present the key properties which were used.

A lot of the properties are similar between IFBA rods and regular rods, a number of these parameters are shown in table 3.4. The coolant flow and inlet temperature were set based on the typical temperatures for a PWR. The fuel properties listed here, porosity, number of cracks, end of densification and porosity after densification are approximate values provided by Westinghouse.

In table 3.5 the key differing properties describing the IFBA and regular rods are shown. The most notable difference here is the initial fill gas pressure and fuel height, both of which are reduced for the IFBA rod to accommodate the helium produced by the IFBA coating. The fill-gas pressures are based on Westinghouse provided typical values. The modification of the fuel stack and plenum height is based on the annular topmost fuel pellets which are normally used on IFBA rods to make room for helium. The size of this additional volume was obtained by trial-and-error here, shifting the fuel stack and plenum height until ZrB_2 gave 7 MPa before fission gas release. Additionally the friction coefficients were modified to account for recent, as of yet unpublished, experimental observations on the fuel-clad bond in IFBA rods. It has been observed that the fuel-clad bond is much weaker for IFBA rods than normal rods.

Table 3.4: The table shows common properties of the non-IFBA and IFBA fuel rod modelled in Transuranus, including the spatial discretization, coolant properties, and some key fuel parameters. The extra axial zone is the upper plenum, and the radial zones in parenthesis describe the cladding.

Property	Value	Unit
Axial Zones	10 + 1	n/a
Coarse Radial Zones	5(1)	n/a
Fine Radial Zones	8(9)	n/a
Coolant Flow	0.2844	kg/s
Inlet Temperature	568.0	K
Initial Porosity	0.05	n/a
End of Densification	13.5	MWd/kgU
Porosity after Densification	0.044	n/a
Initial Number of Cracks	5	n/a

3.2.2 Conversion of Serpent Results

To utilize the Serpent results as input to Transuranus some assumptions were required due to the simplified 2D-geometry used in Serpent. This means that the Serpent results correspond to the axial average over the rod. However, it is possible to rescale the fast neutron flux and linear heat rating to obtain values along the entire rod by assuming a parabolic axial power distribution. Note that the fast neutron flux is approximately proportional to the linear heat rating. The assumed axial distribution used here is:

$$P(z) = \frac{2\bar{P}}{H}(1 - 0.3z^2) \quad (3.2)$$

with the axial coordinate z in mm, H is the height of the rod and the average linear heat rating \bar{P} . Note: $z = 0$ corresponds to the midpoint of the rod.

The second assumption which needs to be noted is the power history. The power history has a large effect on the behaviour of a fuel rod, especially at higher burnup. The neutronics calculations were based on a constant assembly wide normalization of 1728 W cm^{-1} (192 W/cm rod). This is how normalization is typically done for neutronics calculations as the result can be renormalized after.

The input to Transuranus was renormalized with a linearly decreasing power after 40 MWd/kgU , down to 80 MWd/kgU . This a lot smoother than is typically observed for real rods. Under real-world operation fuel rods will experience reactor stops, power ramps and transients. However, it works

Table 3.5: The table shows the key properties of the fuel supplied to Transuranus.

Property	Regular	w/IFBA	Unit
Fuel Stack Height	3800	3720	mm
Plenum Height	360	440	mm
Initial Fill Gas Pressure	1.7	0.7	MPa
Fuel-Cladding Static Friction	0.5	0.01	n/a
Fuel-Cladding Sliding Friction	0.5	0.01	n/a

as an approximation and will produce comparable results. A sensitivity analysis was performed select how low the power should be at 80 MWd/kgU and investigate how sensitive the results are to the assumed power profile.

The modified power history complicates the use of the radial power distribution from Serpent. The Serpent output is only provided at discrete burnup values, with a different power history the burnup needs to be recalculated. Cubic interpolation was used to match the burnup from the redefined power history to the burnup from Serpent. The radial power distribution should be directly related to the depletion of the fuel, which from pure neutronics perspective is only a function of burnup. It should be noted here that Transuranus has models for the radial power profile which incorporate more interactions than Serpent's pure neutronics. The impact this has was investigated by comparing a regular rod with a power profile from Serpent and the recommended Transuranus model called TUBRNP.

3.2.3 Modelling IFBA Gas Production

Transuranus has built in models for modelling gas production in IFBA coatings, however, these are only designed to model standard IFBA coatings. For this thesis a new model was therefore implemented to read the helium production from Serpent and add it to the gas inventory in the free volume in Transuranus. This leverages Transuranus built-in pressure solvers to handle the helium along with any other effects the increased pressure has on the rod.

It was decided to use the cumulative helium production from Serpent instead of the production rate to avoid time integration in Transuranus. Due to the architecture of Transuranus, and specifically where the IFBA routines are called only the current time-step and length of the previous time-step is accessible. This restriction makes time-integration at runtime difficult, and error prone. A less error prone, and more accurate solution than performing time integration at runtime is to pre-compute the cumulative helium

production and use that as the input for Transuranus.

To make it possible to use a modified power history, compared to the constant power normalization used in Serpent, the cumulative helium production was read as a function of rod average burnup instead of time. Regardless of power history the helium produced from the IFBA coating is a function of cumulative flux through the coating, which in turn should be proportional to the burnup. The rod average burnup is computed by Transuranus, and can therefore be used to obtain the cumulative helium production from the Serpent data.

Transuranus uses adaptive time-step sizes, interpolation was therefore required to obtain the helium production at the burnup values observed in Transuranus. A linear interpolation subroutine was implemented for this purpose. From the cumulative helium production, helium could then be added to the free volume inventory every time step. The increment ΔN_{He}^i was calculated as:²

$$\Delta N_{\text{He}}^i = H_{\text{fuel}} \bar{n}_{\text{He}}(B^i) - N_{\text{He}}^{i-1} \quad (3.3)$$

where \bar{n}_{He} is the axially averaged cumulative linear helium density from Serpent, B^i is the rod average burnup at the current time-step, N_{He}^{i-1} is the helium produced up to the previous time-step in Transuranus, and H_{fuel} is the height of the fuel (the entire fuel stack is assumed to be coated in IFBA).

²The upper index in this equation is the time index, not exponent.

Chapter 4

Results

This section will present the main results and observations made from the simulations. Similarly to the methodology it will be broken down into neutronics results (section 4.1) and fuel performance results (section 4.2). Some additional figures not strictly useful for the present aim will be available in appendix A, should they be of use to the reader.

4.1 Neutronics

The first key result from Serpent is the plot of the effective multiplication factor, k_{eff} , and reactivity worth as a function of burnup. To establish the general behaviour of IFBA, Gadolina IBA and normal fuel rods (NOBA) figure 4.1 was produced. The left figure shows k_{eff} , from which a significantly stronger effect is observed from Gadolina Rods than the IFBA rod. This effect is even more clearly visible when looking at the reactivity worth in figure 4.1b. Especially notable in figure 4.1b is the much higher residual reactivity penalty for the IBA rods, and the essentially non-existent penalty for the standard IFBA coating.

With a general idea of the evolution of the reactivity the behaviour of the alternative IFBA coatings can now be studied. Figure 4.2 shows the reactivity worth for the different IFBA candidates demonstrating a broad range of behaviours. Two separate plots are used here for legibility reasons, there is no meaning behind the separation.

Starting with figure 4.2b we can note the very high initial penalty followed by a quick drop off for CdO, GdB₆ and SmB₆, with CdO particularly extreme. Furthermore the two compounds, HfB₂ and GdB₆, show significant residual reactivity penalties. Figure 4.2a does not show any compounds with very quick burnouts and strong initial reactivity, as was observed in figure 4.2b. Two of the compounds, EuB₆ and DyB₆, burn very slowly and therefore produce notable reactivity penalties. To give a clearer overview of the residual reactivity penalty a bar chart of the reactivity penalty at 60

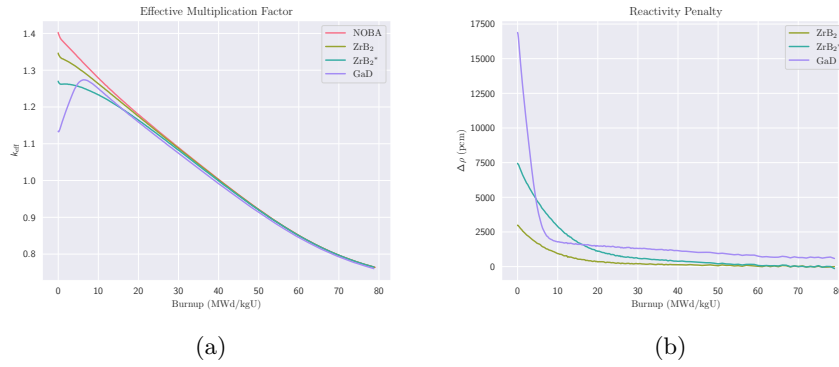


Figure 4.1: The figure shows the evolution of k_{eff} (a) and reactivity worth (b) as a function of burnup for a regular rod, a rod with ZrB₂ IFBA (normal and enriched boron) and a Gadolina IBA rod.

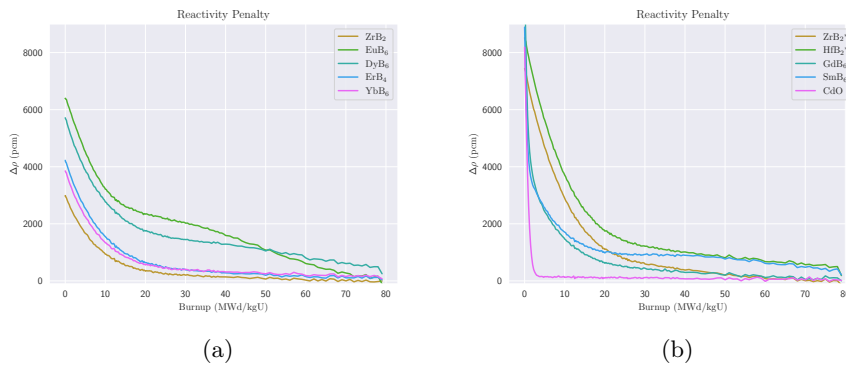


Figure 4.2: The figures shows the reactivity worth as a function of burnup for the IFBA candidates.

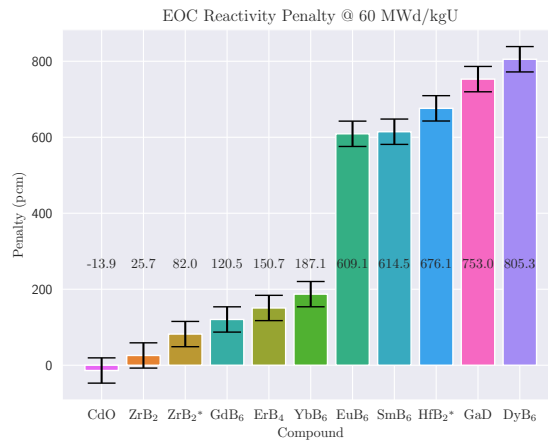


Figure 4.3: The bar chart shows the residual reactivity penalty for each of the candidate compounds, alongside the two tested gadolina IBA rods, at 60 MWd/kgU.

MWd/kgU was put together in figure 4.3.

The europium based compound EuB₆ behaviour is particularly notable from figure 4.2a. It seemingly burns in two stages, with a higher burnrate below 20 MWd/kgU, followed by a plateau at 20-35 MWd/kgU and a slow depletion thereafter.

4.1.1 Capture rate & ^4He Production

The capture rate plot shown in figure 4.4, is quite similar to figure 4.2 of the reactivity penalty. The inflection points in the plot of the capture rate are however ever so slightly earlier, i.e. at lower burnup, than the reactivity penalty, and there is slightly less “noise” in the plot.

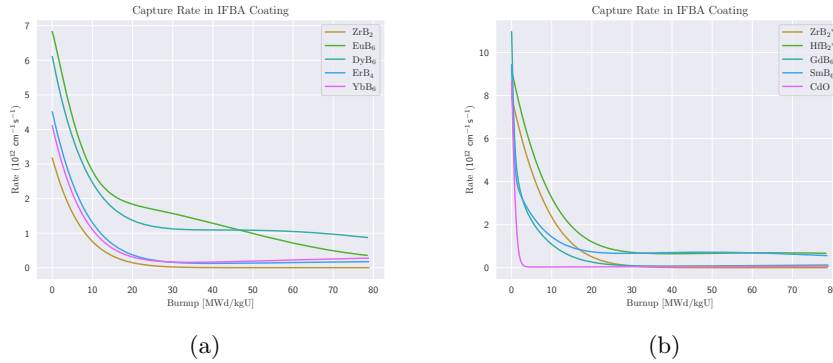


Figure 4.4: The figures show the absolute capture in the IFBA coating for each of the candidate compounds.

The helium production is shown in two ways here, first the helium production rate is shown as a function of burnup in figure 4.5, additionally, the total helium produced in by each of the IFBA coatings is also shown in figure 4.6. From figure 4.5 it can be seen that the helium production for all boron containing compounds is heavily weighted towards the beginning of the cycle.

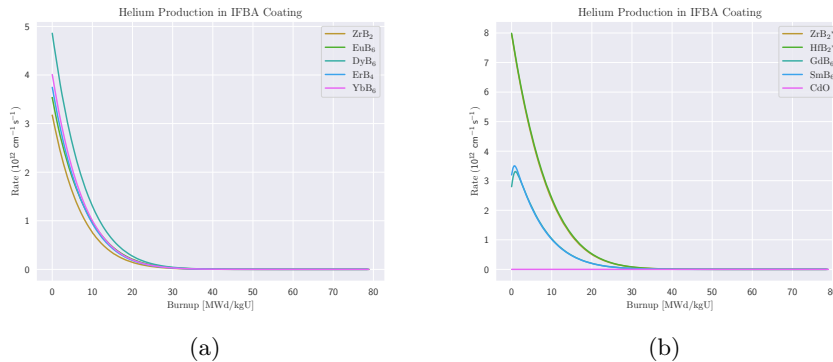


Figure 4.5: The figures show the helium production rate in IFBA coating as a function of burnup for each of the candidate compounds.

To compare the capture and helium production figure 4.7 was produced. This figure shows the fraction of total captures that do not result in helium production. The extreme cases here are represented by ZrB_2 and CdO

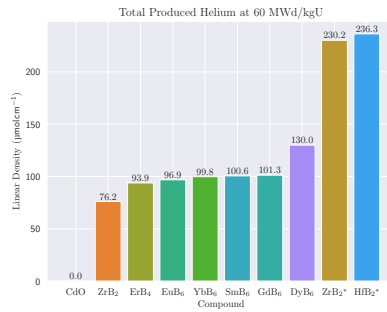


Figure 4.6: The bar chart shows the total helium produced for each of the candidate compounds up to 60 MWd/kgU. Errors omitted as the error is on the order of 0.1 % for all bars.

representing all capture events producing helium and no helium produced at all. All other compounds end up somewhere in the middle, this figure should give some idea of the potential for each of the compounds excluding the specific loading and thickness used here.

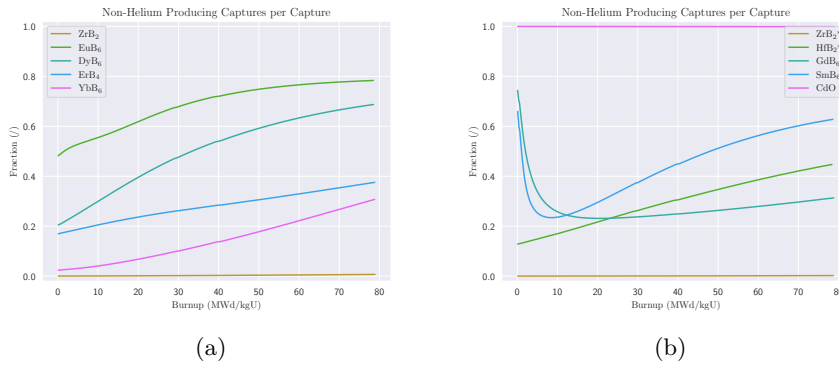


Figure 4.7: The figures show the fraction of total capture events in the IFBA coating that do not result in helium production as a function of burnup.

4.1.2 Local Effects in Fuel

Local effects from the IFBA coatings are mainly observed in the fission rate, and especially the fission rate distribution throughout the fuel. To establish the general behaviour and compare IFBA to a regular and a gadolina IBA rod figure 4.8 was created. This figure shows the very different behaviour of IFBA and IBA. IBA amplifies the parabolic power profile of a standard rod, whilst IFBA flattens the power profile. Also notable here is that the radial power profile converges at higher burnup, qualitatively looking the same at 36 MWd/kgU.

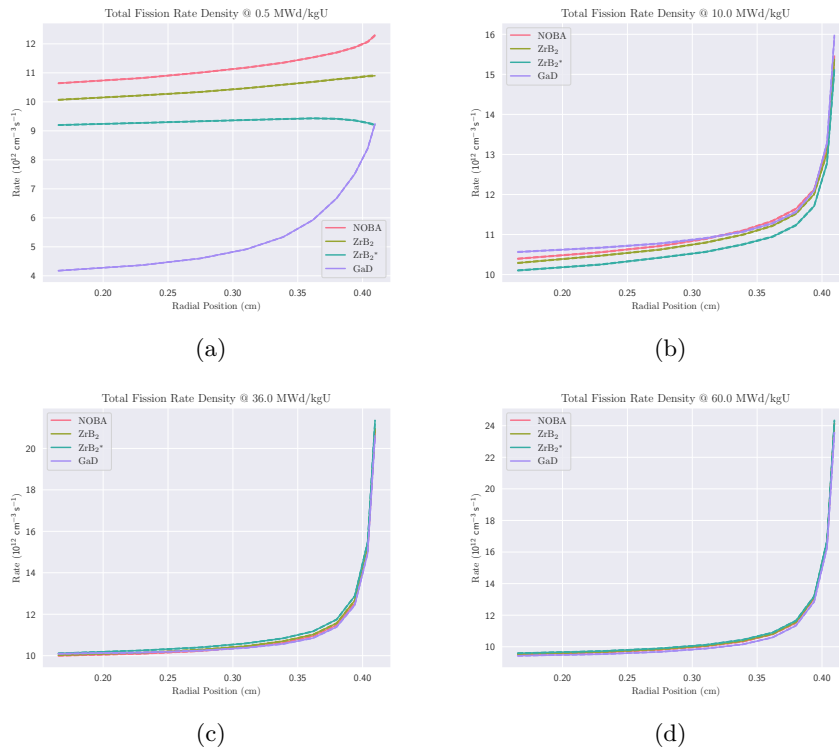


Figure 4.8: The figures show the radial fission rate distribution in the fuel at various burnup for a standard UO_2 rod, a standard IFBA, a boron enriched IFBA rod and a gadolina IBA rod.

Looking at the distribution in a different way the local burnup at the rim as a fraction of rod average burnup can be computed as a function of burnup, this is shown in figure 4.9. Figure 4.9a clearly highlights the previously observed difference, with IBA amplifying the rimward local burnup and IFBA suppressing it. The figures of the IFBA candidate compounds, fig. 4.9b and 4.9c, show that the rimward suppression is present for all candidates, and appears to be largely a function of the absorber strength. The highest local suppression towards the rim largely aligns with the highest capture rate in

the coating.

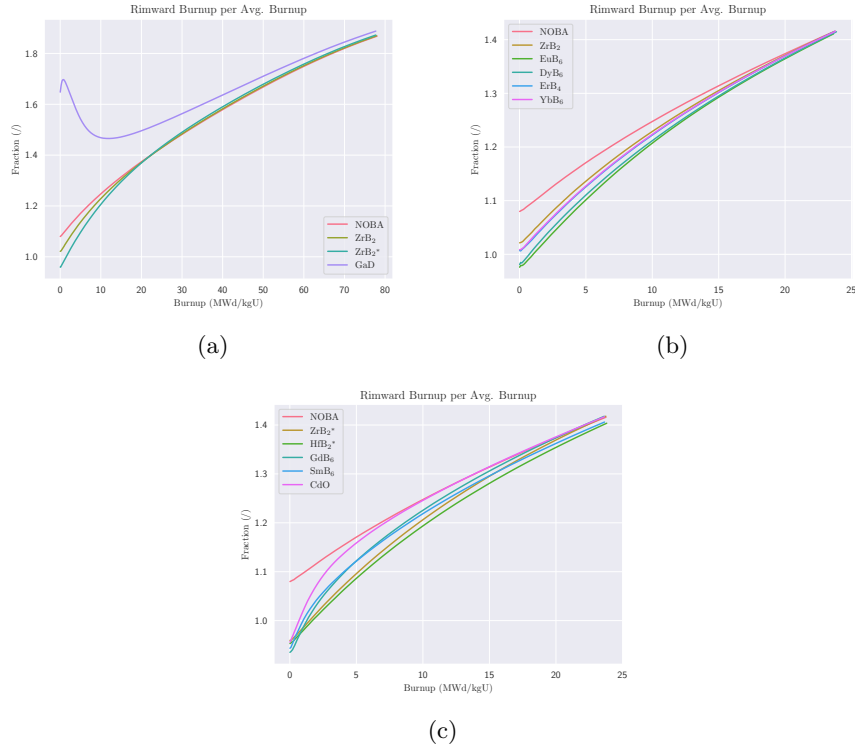


Figure 4.9: The figures show local burnup at the rim as a fraction of rod average burnup as a function of rod average burnup. The figures with the IFBA candidate compounds, b and c, are limited to 24 MWd/kgU to make the differences easier to see.

4.1.3 Xenon Concentration

The Xenon concentration, specifically ^{135}Xe , concentration was also tracked for each of the rods. Figure 4.10 shows the xenon concentration in the fuel as a function of burnup. All the burnable absorbers lead to higher xenon concentration while the burnable absorber is active, with the IBA producing the strongest effect. Notably the xenon concentration for the IBA rod becomes lower than the regular rod after the gadolima is consumed, this does not appear to be happening with the IFBA rod.

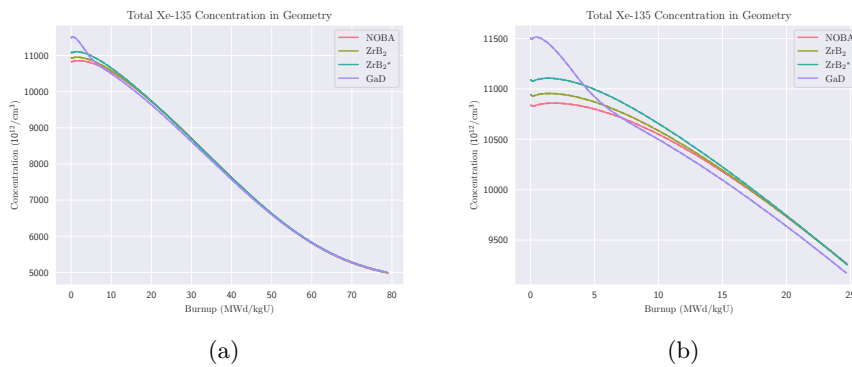


Figure 4.10: The figure shows the Xenon-135 concentration in the entire geometry as a function of burnup for a regular rod, a standard IFBA rod and two different IBA loadings. Figure (a) shows it up to 80 MWd/kgU, and (b) shows it up to 25 MWd/kgU to make the differences easier to see.

Figure 4.11 shows the xenon concentration as a function of burnup for the IFBA coating candidates, showing largely similar behaviour to the normal IFBA rod. The concentration for all coatings slowly converge towards the BA-free rod, with coatings with higher absorption deviating more from the BA-free rod.

4.1.4 Uranium-235 and Plutonium-239 Concentration

The uranium depletion rate as a function of burnup can be seen in figure 4.12 for the base case with a regular rod, standard IFBA and gadolima IBA. This shows a substantially similar behaviour between the four cases, with slightly lower initial concentration for IBA rods initially. In an attempt to ascertain any differences, the difference to the regular rod was computed for each of the IFBA coating candidates. This produced figure 4.13, showing an interesting behaviour with a maximum around 30-40 MWd/kgU for all candidates.

In figure 4.14 the plutonium concentration as a function of burnup for the base case is shown. The notable difference here is the slightly different production rates for the BA rods compared to the BA-free rod. Both IFBA

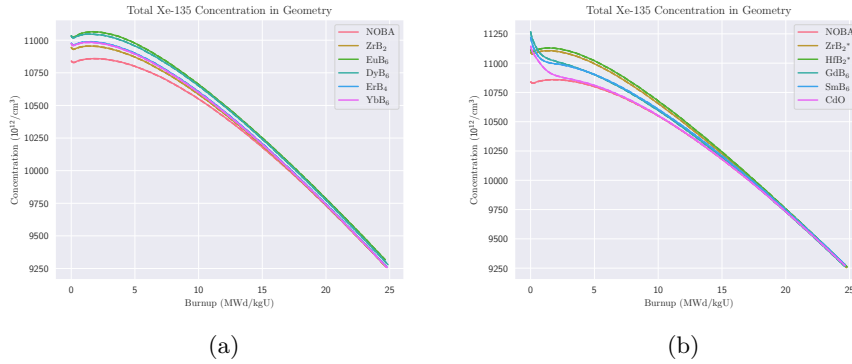


Figure 4.11: Xenon-135 concentration in the entire simulated geometry for each IFBA candidate as a function of burnup.

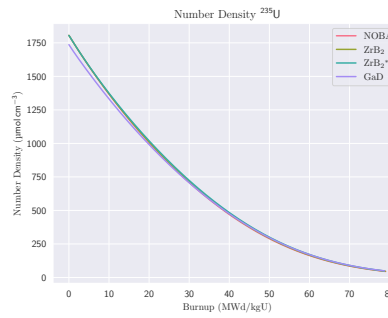


Figure 4.12: The figure shows the number density of uranium-235 as a function of burnup for a regular rod, an IBA rod, a standard IFBA rod and an IFBA rod with enriched boron.

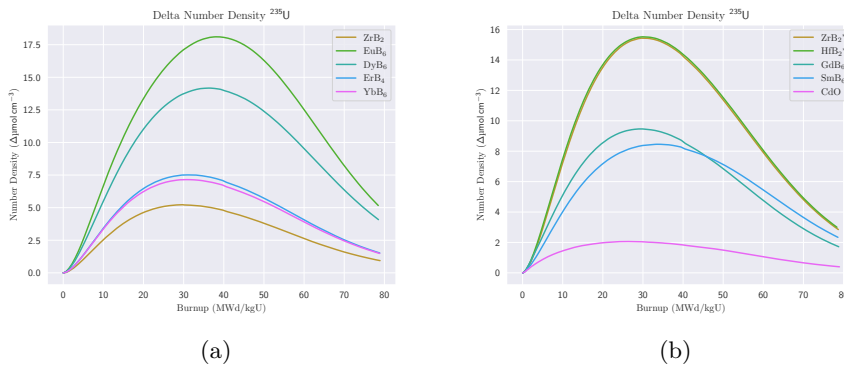


Figure 4.13: The figures show the difference in uranium-235 concentration compared to a regular fuel rod for the IFBA candidate compounds as a function of burnup.

and IBA seem to cause slightly faster production in while they are active. There also appears to be slightly lower EOC concentration for the IBA rods.

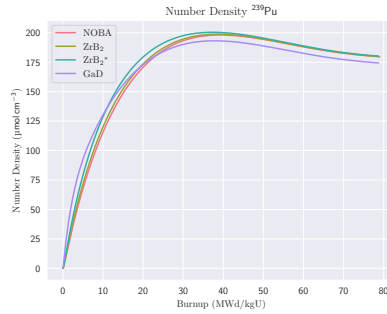


Figure 4.14: The figure shows the number density of plutonium-239 in the fuel for a regular rod, an IBA rod, a standard IFBA rod and an IFBA rod with enriched boron.

Turning to the IFBA candidate compounds, the difference to a BA-free rod can be computed again and plotted in figure 4.15. This produces a peak similar to what was observed in figure 4.13 for uranium-235, however, the peak in the difference in plutonium concentration seems to align closer with the absorber burnout at ~ 10 MWd/kgU.

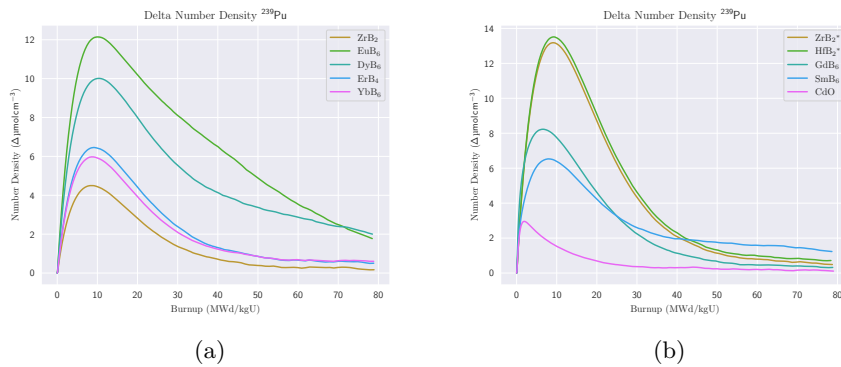


Figure 4.15: The figures show the difference in Plutonium-239 concentration compared to a regular fuel rod for the IFBA candidate compounds as a function of burnup.

4.2 Fuel Performance

This section describes the validation results from Transuranus, alongside the results for the various candidate coatings. Note that the plots shown here are for a single axial zone, the midpoint of the rod, unless otherwise specified.

4.2.1 Power History Sensitivity Analysis

A range of different power histories were compared to investigate the sensitivity to the assumed power history. The result of this is figure 4.16a, showing a variety of linear power reductions at the end of life. In the figure the linear profiles reduce power linearly after 40 MWd/kgU to 75-100 % at 80 MWd/kgU. Note that the simulations are terminated at 65 MWd/kgU.

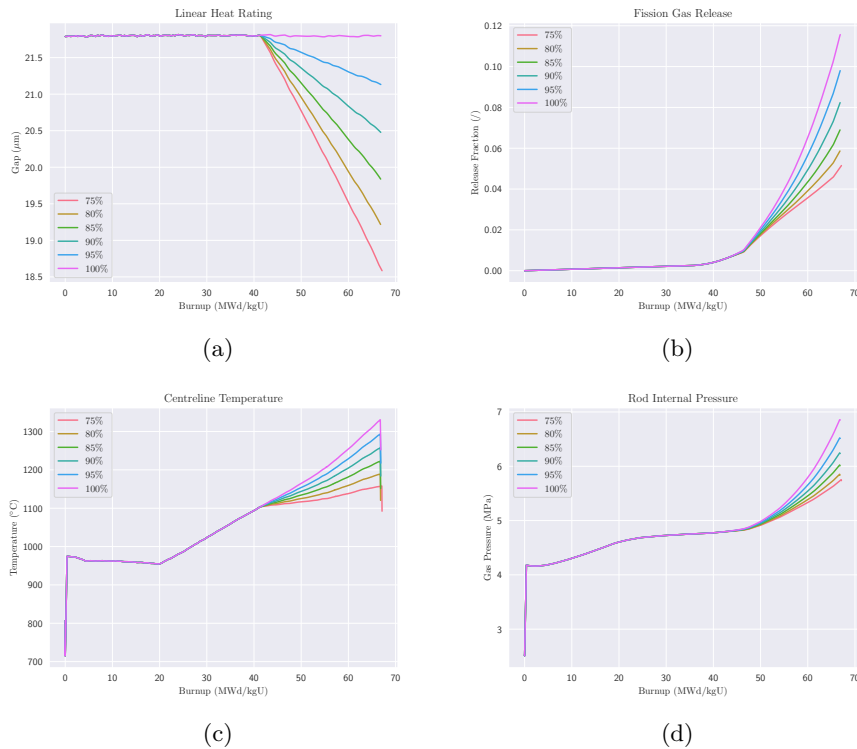


Figure 4.16: The figure compares a couple of key properties with different power histories. The power histories tested are shown in (a), the fission gas release is shown in (b), along with centreline temperature (c) and rod internal pressure (d)

The effect of a higher linear heat rating is visible in all three properties monitored in figure 4.16. The centreline temperature increases at end of cycle, as seen in figure 4.16c, peaking at ~ 1320 °C at constant full power and

~ 1150 °C with the power history terminating at 75 % power. An effect of a similar scale is seen on both the fission gas release (fig. 4.16b) and the rod internal pressure (fig. 4.16d). Qualitatively the behaviour appears similar aside from the different rate of change for the different power histories.

4.2.2 Radial Power Profile Validation

The radial power profile read from Serpent for a standard non-IFBA rod was compared to the built in model recommended by Transuranus for PWR rods. A direct comparison of the power profile at rod average burnup 1, 10, 30 and 60 MWd/kgU is available in figure 4.17. In figure 4.17a the difference between the two radial power profiles is quite small, with the Serpent profile having a slight deficit towards the rim and a slight surplus towards the centre. The difference is larger at 4.17b, however, it does not seem to grow markedly after that.

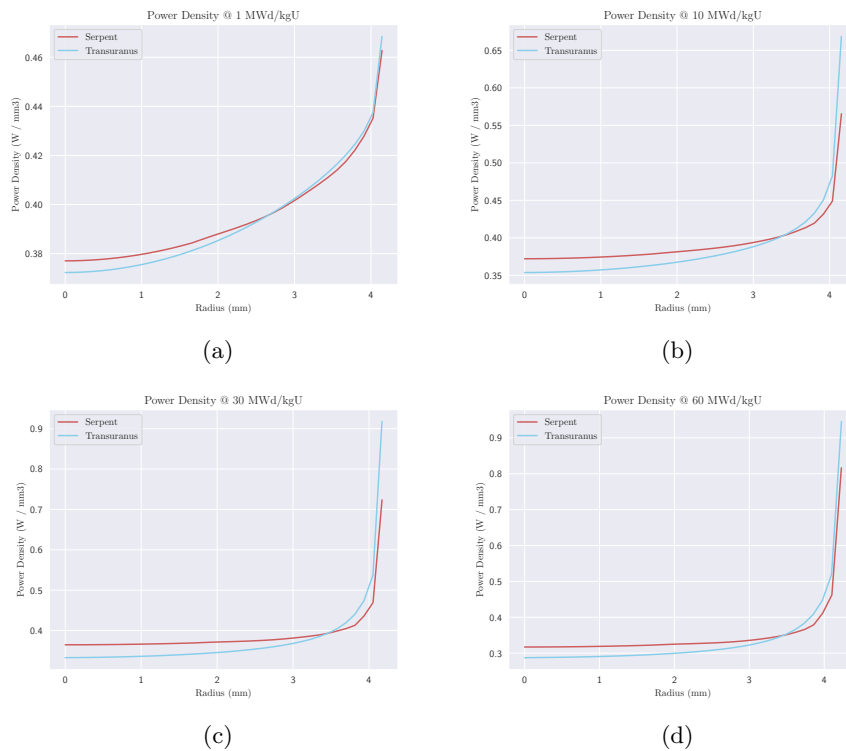


Figure 4.17: The figures show the power distribution at various burnup steps.

To monitor for secondary effects, figure 4.18 was produced showing a range of rod properties at the midpoint axially. Figure 4.18a shows the centreline and surface temperature, 4.18b fission gas release, 4.18c rod internal pressure and 4.18d shows the free volume evolution. Overall the

two models agree very well, the only notable differences are slightly higher centreline temperatures, slightly delayed and slightly lower internal pressure.

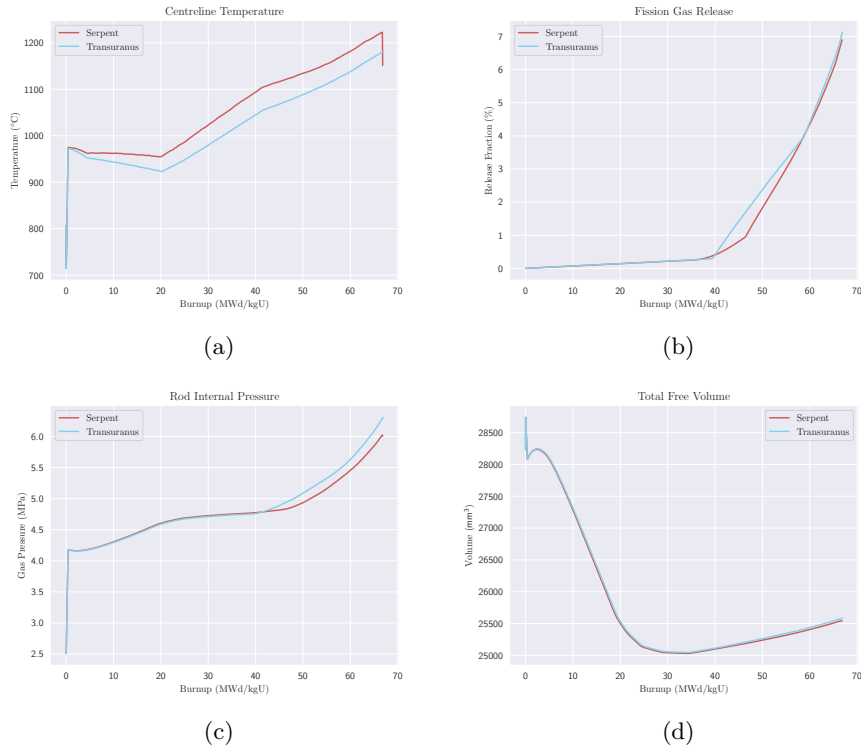


Figure 4.18: The figure compares a regular fuel rod with a radial power profile from Serpent against the recommended power profile from Transuranus. The subfigures show (a) the centreline and surface temperature, (b) fission gas release, (c) rod internal pressure, (d) free volume evolution.

4.2.3 IFBA Gas Release Validation

To ensure that the implemented IFBA gas release model worked correctly the linear gas release was compared between the Serpent result and Transuranus. Figure 4.19 shows the result of this for a standard ZrB_2 IFBA rod, with very good agreement.

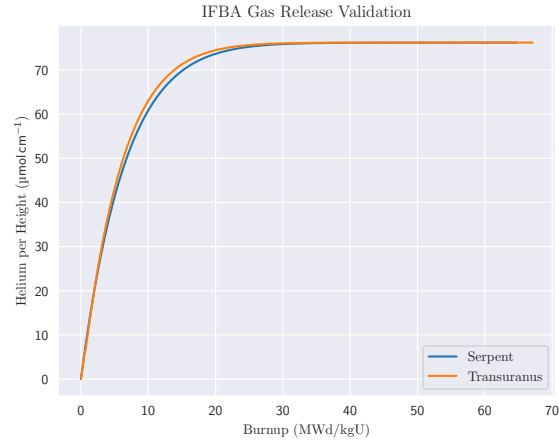


Figure 4.19: A comparison between the produced axially averaged helium per height between the Transuranus model and Serpent.

4.2.4 Results for Alternative IFBA Compounds

The linear heat rating after applying a ramp down towards the end of the cycle for each of the IFBA compounds can be found in figure 4.20. Notably missing here is ZrB_2^* and HfB_2^* , these produce too high pressures and have therefore been excluded.

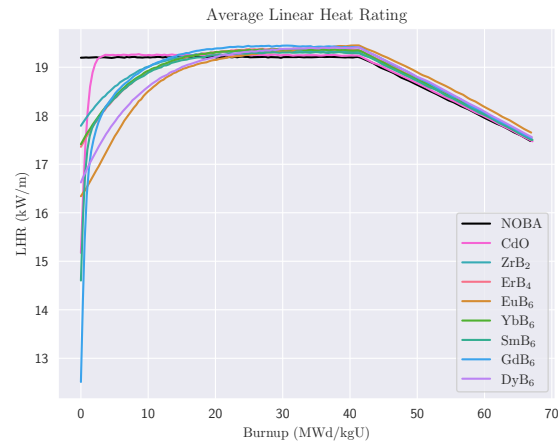


Figure 4.20: The figure shows the linear heat rating used as a function of rod-average burnup for the different alternative IFBA compounds.

The first set of results from Transuranus for the different IFBA coatings are available in figure 4.21. This figure shows the centreline, surface and plenum temperature as functions of burnup, alongside the rod internal

pressure, total free volume, and cumulative helium release from the IFBA coating.

Subfigure 4.21a, 4.21b and 4.21c show the centreline, fuel surface and upper plenum temperature, respectively, for rods with the different coatings. The general behaviour for all alternative IFBA coatings is similar:

- The centreline temperature at first increases slowly, followed by an inflection to a slightly steeper increase.
- The surface temperature initially drops approximately linearly, followed by a constant temperature.
- The plenum temperature is constant.

The different coatings generally exhibit the same temperatures. However, there are small differences for ZrB_2 and DyB_6 . ZrB_2 has slightly lower surface temperatures initially, and slightly steeper initial decline. DyB_6 has slightly higher surface temperatures, and a slightly slower initial decline. Both converge to the same value after the initial decline in surface temperature.

The rod internal pressure is shown in figure 4.21d shows an initially steep pressure increase followed by a plateau at 25 MWd/kgU, followed by a gradual pressure increase again around 50 MWd/kgU. The general behaviour is similar between the different coatings, however the absolute pressure varies greatly. The bar chart in figure 4.22 highlights this by showing the pressure at 40 MWd/kgU, in the middle of the plateau.

Figure 4.21e shows the free volume evolution inside the cladding. This figure shows a small initial increase in volume followed by a large decrease only ending around ~ 35 MWd/kgU. Finally there is a small increase after ~ 35 MWd/kgU. All coatings generally behave similarly here, however, ZrB_2 is slightly ahead, with an earlier and slightly steeper decrease in volume. DyB_6 is the opposite, with a slightly less steep, and slightly delayed drop.

Figure 4.23 shows the radial temperature distribution in the fuel rod at various rod average burnups. Overall there are very small differences in temperature here, with the largest deviation at 1 MWd/kgU being a spread of ~ 50 °C between the hottest candidate and the coolest at the centreline.

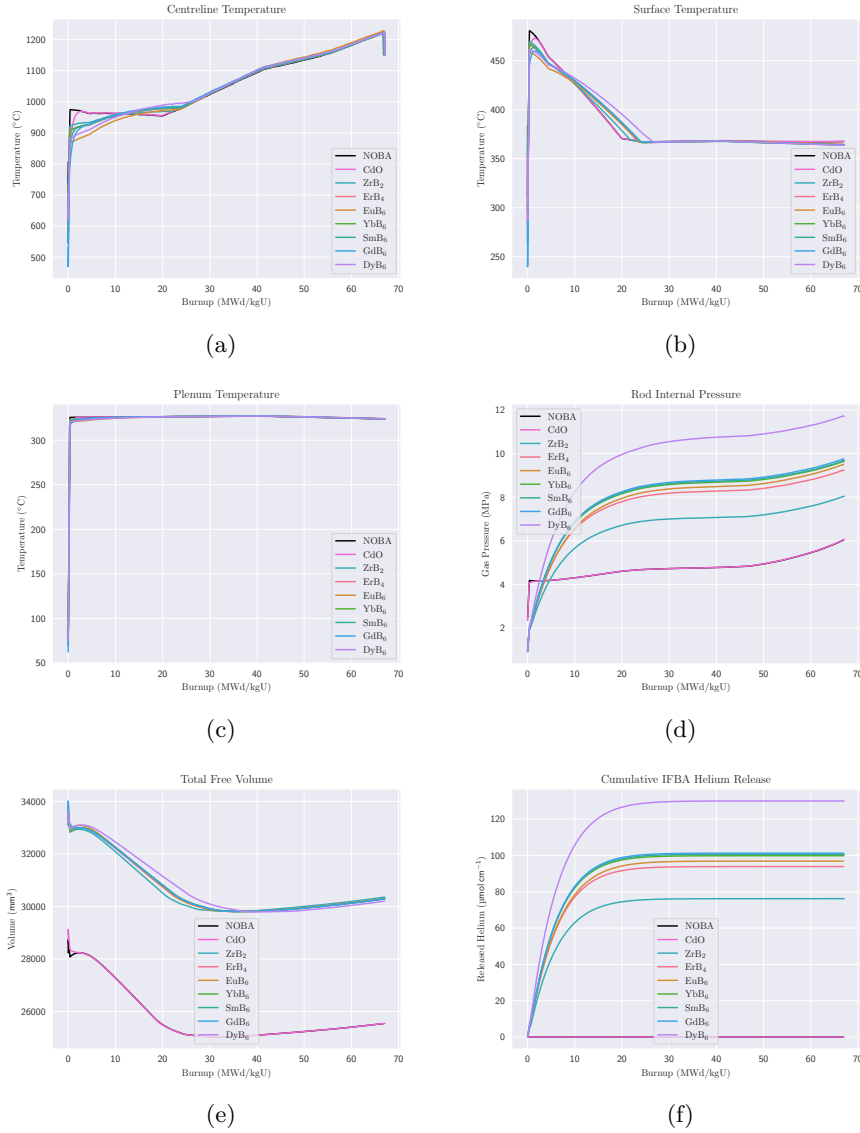


Figure 4.21: The figure compare a range of fuel performance characteristics between the various IFBA candidates. In the subfigures the following quantities are shown as functions of burnup: (a) centreline temperature, (b) fuel surface temperature (c) plenum temperature, (d) rod internal pressure, (e) total free volume and (f) cumulative IFBA helium production.

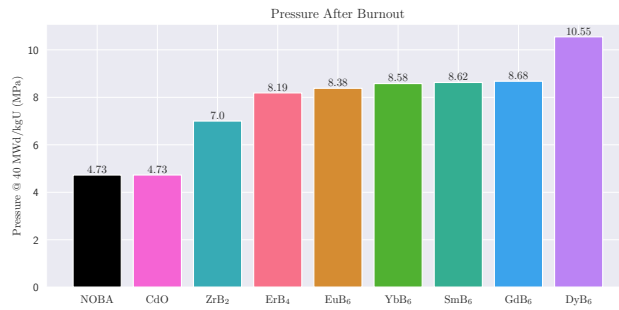


Figure 4.22: The figure shows a bar chart with the rod internal pressure for IFBA rods with the various coatings at 40 MWd/kgU.

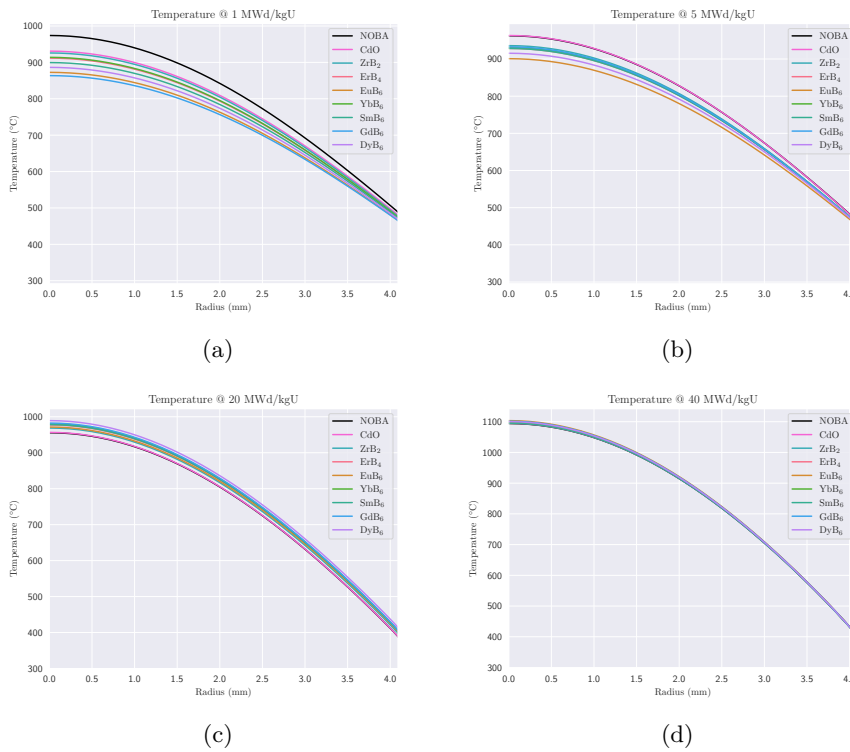


Figure 4.23: The figures show the power distribution at various burnup steps.

Chapter 5

Discussion

This chapter will start by discussing general observations on IFBA and IBA from the neutronics results. This will be followed by a deep dive comparing the considered alternative coatings based on the neutronics results. Finally fuel performance will be discussed, with a discussion on the validity of the Transuranus results followed by a discussion of the results for the alternative IFBA coatings.

5.1 Neutronics of IFBA and IBA

The results presented above show gadolima IBA alongside standard ZrB_2 and boron enriched ZrB_2 IFBA rods. Since IBA is the main competitor to IFBA for extended cycles it will prove an instructive comparison for discussing general trends.

The first notable difference between IFBA and IBA is the much higher reactivity worth of the IBA rods, as shown in figure 4.1b. This has the direct consequence that fewer IBA rods are needed to achieve a certain reactivity suppression. Fewer BA rods could potentially be beneficial from a cost perspective as fewer specialized rods are needed, but this would depend on the precise cost of IFBA and IBA rods. Fewer BA rods does however have downsides from a core design perspective. Using a few very strong absorbers can lead to power peaking, and stronger absorbers therefore carry more constraints than weaker absorbers. Many IFBA rods can distribute the reactivity suppression more effectively, creating a smoother power distribution and offering more flexibility.

Another notable difference is the burnout characteristics: the IBA rods burn out much sooner than the standard ZrB_2 IFBA rods. However, it is difficult to declare this a positive or negative, both are within a range which could be seen as desirable depending on the specific core design. The more significant difference here is the much higher residual reactivity penalty for the IBA rods compared to IFBA, as seen in figure 4.3. This is a clear benefit

of the IFBA rods, the reactivity penalty for a burnable absorber should be as low as possible as it reduces fuel efficiency. At high burnup there is no reactivity excess that needs to be suppressed, quite the opposite, the residual reactivity penalty hurts the neutron economy.

Whilst there was not time to perform calculations for the IBA rods in Transuranus, some information can be extrapolated from the Serpent results. Of particular interest is the radial fission rate distribution, figure 4.8 shows that the two rod types produce radically different fission rate distributions. It seems that the IBA rods exacerbate the power profile of the normal rods, further increasing the power concentration at the rim. This could increase risks associated with e.g. FFRD, as those risks are largely a function of local burnup. The initially flattened power distribution for IFBA rods should have the opposite effect, potentially reducing risks associated with FFRD, potentially increasing safety margins. However, post irradiation examination would likely be required to determine the significance of these differences.

Another important comparison is the evolution of ^{235}U and ^{239}Pu concentration. The evolution of uranium-235 concentration is largely the same, aside from the small deficit in the IBA rods due to the replacement of uranium with gadolima as is seen in figure 4.12.

The ^{239}Pu concentration is slightly more interesting, it appears that the presence of burnable absorbers, regardless of type, promotes plutonium production. Both the IBA and IFBA rods produce plutonium slightly faster than the regular rod, but converge with the BA-free rod after the absorber is consumed. The explanation for this likely lies in the cross-section for the $^{238}\text{U}(n, \gamma)$ reaction, ^{239}Pu is produced through two sequential beta-decays of ^{239}U . Figure 2.3 shows that the cross-section is the highest at the resonances. Boron has its highest absorption cross-section at thermal energies. The burnable absorber will therefore suppress the fission rate (predominantly thermal flux-driven) more than the ^{239}Pu production rate.

Curiously the IBA rod ends up with a slightly lower plutonium concentration in the end than the IFBA rod. The most plausible explanation seems to be the slightly lower uranium concentration due to the $\text{UO}_2\text{-Gd}_2\text{O}_3$ solid solution. It is possible that this reduction in plutonium concentration contributes slightly to the residual reactivity penalty of the IBA rods.

5.2 Neutronics of Alternative IFBA Coatings

Considering the neutronics results for the alternative IFBA coatings, and starting with reactivity worth, figure 4.2. From the general shape of the curves it will prove useful to divide the candidates into four groups:

- ZrB₂-like: ErB₄, YbB₆ and DyB₆

- Black: GdB_6 , SmB_6 and CdO
- EuB_6
- Enriched Borides: HfB_2^* and ZrB_2^*

Each of these groups will be described and discussed in detail in the subsequent subsections.

5.2.1 ErB_4 , YbB_6 and DyB_6

The compounds ErB_4 , YbB_6 and DyB_6 exhibit a similar evolution of the reactivity worth over time as ZrB_2 , with a smooth exponential decay of a relatively moderate reactivity worth. This should make them viable as drop-in replacements for ZrB_2 , with largely the same design considerations from a neutronics perspective. The IFBA rod placement and neighbouring uranium enrichment should largely be the same as for ZrB_2 , if the thickness is reduced to provide an equivalent reactivity worth.

However, notable here is the high residual reactivity penalty of DyB_6 , see figure 4.3, over ten times higher than ZrB_2 effectively eliminating it from consideration. The other two compounds, ErB_4 and YbB_6 , each have slightly higher residual reactivity penalty. However, as they are slightly stronger absorbers than ZrB_2 this might be acceptable depending on their helium production.

Turning to the helium production, both ErB_4 and YbB_6 produce slightly more helium than ZrB_2 . However, keeping in mind that both are slightly stronger absorbers when using the same coating thickness, figure 4.7 becomes useful for evaluating their potential with reduced thickness. Both compounds have a non-zero fraction of non-helium producing captures, should the reactivity worth be adjusted by reducing the coating thickness both should have a lower boron loading than ZrB_2 . A lower boron loading equates to lower helium production.

Additionally, ErB_4 has significantly more non-helium producing captures than YbB_6 based on figure 4.7. This implies that ErB_4 could provide the same reactivity worth with a lower helium production. Alternatively, ErB_4 could provide the same helium production and a higher reactivity worth. This could allow for core designs with even higher enrichments or reduce the number of required IFBA rods.

As one might expect for compounds with similar reactivity worths and depletion profiles, the compounds are also similar in other respects. There are no major differences in the local power suppression, the xenon-135, uranium-235 or plutonium-239 concentrations. The slightly higher reactivity worth seems to amplify the observed effects slightly, but otherwise behave very similarly to ZrB_2 . Further supporting that they could be drop-in replacements.

5.2.2 GdB₆, SmB₆ and CdO

The strongest absorbers GdB₆, SmB₆ and CdO deplete very quickly, as can be seen from the rapid initial drop in reactivity worth in figure 4.2. These compounds exhibit very different behaviour from ZrB₂, their reactivity worth evolution is more akin to the gadolinia IBA rods than standard IFBA. The initial reactivity worth is however quite a bit lower than IBA. Potentially this could offer additional flexibility in core design compared to IBA rods, e.g. allowing for more rods to create a smoother power distribution.

However, the quick burnout of cadmium oxide, CdO, is likely a little too extreme in this regard. It is difficult to argue the period for which it suppresses reactivity (~ 2.5 MWd/kgU) constitutes long-term reactivity control, which is the point of burnable absorbers. In spite of its non-existent residual reactivity penalty and zero helium production it is not suitable for this application. Likely it would need to be used in much larger quantities than is feasible in IFBA rods. Even this might be problematic due to the high cross-section causing excessive reactivity suppression.

The other two compounds in this group, GdB₆ and SmB₆ do have residual reactivity penalties and helium production. The residual reactivity penalty for SmB₆ is likely too high for it to be attractive as a burnable absorber, GdB₆ on the other hand is notable but not that significant. Figure 4.7 also indicates that GdB₆ hovers around 20 % non-helium producing captures, which is a decent improvement over ZrB₂. Out of this group GdB₆ is certainly the best alternative, though the very different depletion profile could make it difficult to use as a drop-in replacement for ZrB₂. Future research would be needed to determine if the different depletion profile is desirable, likely involving a deep dive into core-loading schemes.

5.2.3 EuB₆

Europium Hexaboride has some unique depletion characteristics, it appears to deplete in two “stages”. This can be seen in figures 4.2 and 4.4, initially there is a quite steep drop in the reactivity worth, and capture rate, up to ~ 20 MWd/kgU. After 20 MWd/kgU there is a very slow drop up to about ~ 35 MWd/kgU, followed by a steeper decline which eventually completely depletes the absorber. The helium production rate in figure 4.5a shows that the boron is depleted in the first stage. The second stage is either purely europium depletion, with boron initially shielding it slightly, or build-up of another absorber isotope through transmutation.

As expected given the clear two-stage depletion with boron-10 only contributing to the first stage, there is a significant fraction of capture events without any helium production. Based on figure 4.7, only about 50% of the absorption during the first stage produces helium. As the second stage

doesn't produce helium the cumulative fraction grows to about 80 % in the end. Whether the second stage is useful or a penalty is somewhat unclear.

At typical rod average burnup of ~ 60 MWd/kgU the second depletion stage appears quite detrimental, as a significant reactivity penalty remains. However, it is interesting that the reactivity penalty essentially vanishes at ~ 80 MWd/kgU. Given the high initial reactivity worth of 6% there is some margin to reduce the thickness while still offering stronger suppression than ZrB_2 . Since the capture rate decays exponentially, doing so would also reduce the depletion time. Determining the usefulness for core design of a two-stage burnable absorber would require more detailed exploration of the core design implications. However, it would not be a drop-in replacement for ZrB_2 IFBA.

5.2.4 ZrB_2^* and HfB_2^*

The boron-10 enriched compounds ZrB_2^* and HfB_2^* produce a significant amount of helium compared to the standard ZrB_2 , in fact based on figure 4.6 they produce over three times the amount. It is debatable whether this amount of helium could be manageable inside the rod given the challenge of managing the helium produced by standard ZrB_2 . They are however interesting from a more theoretical perspective because of their high reactivity worth and extended active period.

The increased boron-10 loading of these compounds leads to a much higher reactivity worth but also a much longer lifetime. Figure 4.2b shows that these compounds lasts 10 MWd/kgU longer than standard and ZrB_2 . The stronger reactivity worth also amplifies the desirable effect on the local level by increasing the fission rate suppression at the rim and the plutonium-239 production.

Regarding hafnium diboride, whilst only results for enriched boron are included here it is possible to conclude that regardless of boron enrichment it is unsuitable to use as a burnable absorber. The very high residual reactivity penalty observed for HfB_2^* in figure 4.2b can only be from hafnium, as figure 4.5b shows that all helium is produced in the beginning. Given the similar reactivity worth to ZrB_2^* one can fairly confidently hypothesize that HfB_2 would be similar to ZrB_2 but with the same residual reactivity penalty. It thus would not be possible to reduce the thickness to reduce the penalty.

5.3 Transuranus Simulation Accuracy

As a fair number of assumptions and approximations were required for the Transuranus simulations a discussion needs to be had on their impacts. This section will discuss the results shown in sections 4.2.1 - 4.2.3 which test the most major assumptions and IFBA gas release code.

5.3.1 Power History Sensitivity & Fission Gas Release

As is clear from figure 4.16, Transuranus is very sensitive to the power applied to the rods. The linear heat rating has a direct impact on the centreline temperature, this is to be expected as there is more heat which needs to be dissipated. The temperature differences on their own are however not that significant. A more important impact of the power history is the effect on fission gas release, and thereby rod internal pressure. A completely flat power profile leads to 12 % fission gas release, and the most conservative leads to only 5 %. The fission gas release has a large impact on the final pressure in the rod.

A better solution would have been to use the power history for a real fuel rod, this is something that could be explored in future work and would produce more realistic results. With the goal of comparing the fuel performance of different IFBA coatings a synthetic profile which gives “reasonable” fission gas release will suffice. The middle power history was used because of this.

It should also be noted at this stage that the some parts of the fission gas release model in the Transuranus version used here are simplified, and uncertain. Under steady-state operating conditions very little fission gas release occurs at low burnup, just as is observed here. However, at higher burnup, fission gas is thought to release from the high burnup structure, this is the main source of the fission gas release observed here. The mechanics of HBS fission gas release are an active area of research and not fully understood. Transuranus models fission gas release from the HBS as simple burnup threshold, with full release as soon as the local burnup reaches a specific value.

As reactor operators are moving to longer cycles these effects become increasingly important. Given the large amount of gas released at EOC, correctly understanding this is critical for safe operation of fuel to high burnup. HBS fission gas release should be the subject of future research.

5.3.2 Radial Power Profile

The radial power profile from Serpent deviates slightly from the recommended model in Transuranus for a standard PWR rod, as was observed in section 4.2.2. The Transuranus documentation is a little vague on exactly how their model works, it is some form of semi-analytical model based on, likely more detailed, simulation results. There are a couple of ways the observed difference could come about, the two most likely are more power bins and treatment of radial temperature.

Additional bins for the power measurement could produce increased power at the rim simply due to smaller bins towards the rim. The tally of a bin in Serpent corresponds will correspond to the average over the region. Towards

the very rim this could result in reduced peak power due to the sharp increase towards the rim. An alternative approach could be to use functional expansion tallies, this is a new type of detector under development in Serpent which instead of tallying into bins computes coefficients for functional expansions e.g. Zernike polynomials. The result is a continuous function, theoretically this could provide better results here. However, the implementation does not seem entirely complete, or at least the documentation is not, for the version of Serpent used here. In spite of my best efforts I could not get it working.

The temperature profile is another potential explanation. In Serpent the fuel was set to an homogenous temperature of 900 K, the actual surface temperature of the fuel, as seen in e.g. figure 4.23, is quite a lot lower. Neutron cross-sections are temperature dependent, decreasing with temperature. Due to this the power density measured at the rim in Serpent is lower than it should be.

Nevertheless, the results seem to indicate that this difference has a very minor effect on fuel performance. The most notable difference being the at most 50 °C higher centreline temperatures. This difference should be noted, however it is unlikely to have any major impacts on the results.

5.3.3 IFBA Gas Release

The IFBA Gas release subroutine that was developed to read and interpolate the Serpent results appears to work correctly. Figure 4.2.3 shows very good agreement between the IFBA gas released in Transuranus and the Serpent Results. The very small difference seen is likely due to interpolation, but is not going to have any meaningful impact. Especially as the models converge to the same total helium production.

5.4 Fuel Performance of Alternative IFBA Coatings

The fuel performance of the different IFBA compositions is qualitatively the same between all the candidates. Minor differences exist when looking at e.g. the temperature at low burnup in figure 4.23a, the stronger absorbers lead to lower temperatures towards the centre of the fuel. The difference is however very small towards the surface, with only a couple °C separating the compounds. This is a little surprising given the difference in rimward burnup observed in the neutronics results. The heat equation seems to largely smooth out the temperature effect of the local power suppression.

The free volume evolution also differs slightly, with the rod coated in DyB₆ seeing a slower reduction in free volume. Interestingly enough this effect is stronger in DyB₆ than EuB₆, despite EuB₆ suppressing power more

than DyB_6 as seen in figure 4.20. This seems to be caused by the higher rod internal pressure, a slight outward expansion of the cladding would explain the observed effect. The other coatings which produce only slightly more helium than ZrB_2 see a slightly delayed free volume evolution compared to ZrB_2 , seemingly further supporting this explanation. Finally CdO , which sees no helium production, and therefore has the fastest free volume reduction.

The pressures observed here are somewhat high, typical operating pressures for PWR rods are in the range of 6-7 MPa whilst most of the IFBA rods tested here are around 8.5 MPa. This is due to the decision to use the same thickness for all burnable absorbers, in hindsight it likely would have been better to compare the coatings with a thickness determined by the boron loading. It would have produced more realistic pressures and made comparisons easier.

It is difficult to find any meaningful difference in fuel performance between IFBA rods using the alternative compounds. Aside from the different rod internal pressures due to the coatings producing different amounts of helium the performance appears largely equivalent.

5.5 Key Insights & Outlook for IFBA Development

The main goal of this thesis was to find an alternative IFBA coating to ZrB_2 which provides lower helium production whilst maintaining, or improving, the performance improvements a ZrB_2 coating provides. As was highlighted in section 5.1, IFBA has a pronounced impact on early cycle reactivity but notably a smaller impact than IBA. It also provides a slightly flattened early cycle radial power profile, especially compared to IBA, but also regular fuel.

From the neutronic simulations four broad categories were identified, ZrB_2 -like, "black", EuB_6 and Enriched Borides. These categories can be summarized as follows:

- ZrB_2 -like: generally demonstrated smooth exponential decay of reactivity worth, qualitatively similar to ZrB_2 . This group contains ErB_4 , YbB_6 and DyB_6 . In this group ErB_4 seems the most promising due to its low residual reactivity penalty compared to YbB_6 , higher proportion of non-helium producing captures compared to YbB_6 ; though YbB_6 is a close second.
- "black" absorbers: characterized by a strong initial reactivity suppression and rapid depletion. This group contains GdB_6 , SmB_6 and CdO , of which only GdB_6 seems like a remotely viable option. Despite zero helium production CdO burns out too quickly to provide any mean-

ingful long term reactivity control. SmB_6 is similar to GdB_6 , but has a large residual reactivity penalty which makes it unsuitable.

- EuB_6 is unique, it exhibits a two-stage depletion. With boron-10 depleted first, followed by a slower depletion of the Europium. Complete depletion with the thickness simulated came a little too late, however given the strong reactivity suppression the thickness can be decreased quite significantly.
- Enriched Borides: Provided qualitatively similar behaviour to ZrB_2 , but higher reactivity worth, and improved staying power. However, both the compounds in this group use enriched boron, which led to very high helium production. It was also observed for these that HfB_2 (even if not enriched) likely has too high a residual reactivity penalty to be suitable as a burnable absorber.

Out of the above only the ZrB_2 -like absorbers ErB_4 and YbB_6 could potentially function as a drop in replacement for ZrB_2 . The others GdB_6 and EuB_6 would require a large shift in the role of IFBA rods in core design and reactivity control. The most promising replacements are therefore ErB_4 , followed by YbB_6 .

The fuel performance simulations did not alter this picture. It did however highlight the value in finding an alternative to ZrB_2 that reduces helium production. All meaningful differences in fuel performance between the tested compounds were explainable based on the rod internal pressure, to which helium production is the largest contributor in an IFBA rod.

The two main contenders identified, ErB_4 and YbB_6 , are both based on rare-earth elements, and as such the raw material cost is higher for these than ZrB_2 . However, the significance of this will depend on the total cost of manufacturing the compounds and applying the coating to the fuel, this is outside the scope of this thesis and left for future research.

The results of this thesis highlight two main pathways for the development of a replacement for ZrB_2 . The first is further exploration of the most promising candidates ErB_4 and YbB_6 focusing on manufacturability, cost and chemical compatibility with fuel and cladding. The second would be to explore more creative alternatives, potentially focusing on boron-free alternatives given the large and detrimental effects of helium on fuel performance.

For future development of IFBA coatings in a broader sense an interesting avenue could be to explore a “black” absorber like GdB_6 . One might imagine it being used as an even more direct alternative to gadolinia IBA given the similar depletion profiles. However, given the weaker reactivity suppression it could potentially be applied to more rods for a smoother power distribution. Along the same line, a two-stage absorber like EuB_6 could be an interesting area to explore with the burnable absorber thickness, and potentially boron enrichment, adjusted so that the absorber is

active with two different reactivity worths for two cycles.

Chapter 6

Conclusion

This thesis aimed to evaluate alternative materials to the currently used ZrB_2 in integral fuel burnable absorber fuel. The primary goal was to find something with similar or better neutronic performance, whilst reducing helium production. Helium production is seen as the largest hindrance for expanded IFBA use, because it leads to a large increase in pressure in IFBA rods.

Simulation results for a range of different compounds were presented, both neutronics results from Serpent 2 and fuel performance results from Transuranus. This made it possible to assess both neutronic characteristics and thermomechanical effects on the fuel.

Many compounds, such as CdO , SmB_6 , HfB_2 and DyB_6 were found to have critical drawbacks as IFBA coatings. For instance excessively rapid depletion, high residual reactivity penalties or high helium production. However, ErB_4 and YbB_6 were found to have similar reactivity worths and lifetime to ZrB_2 along with acceptable residual reactivity penalties. Compared to ZrB_2 both compounds offer a significant fraction of non-helium producing captures which should give the possibility of similar performance with less helium. With ErB_4 slightly better in this regard, potentially having slightly more room for reducing thickness and thereby total helium production, while maintaining neutronic performance.

An additional two compounds were found to have intriguing characteristics, EuB_6 and GdB_6 , however they both had significantly different depletion characteristics. EuB_6 was observed to be long-lived, have significant fraction of helium-free captures, and a unique two-stage depletion. The other compound, GdB_6 , had depletion characteristics more akin to IBA than IFBA, due to it being a “black” absorber. Exploring the utility of IFBA rods based on these present an interesting avenue for future research, however, they may not be suitable as direct replacements of ZrB_2 .

An important result to highlight from this work is that the only aspect that appears have a meaningful impact on fuel performance was the pressure

from the helium release. The small differences in power distribution between the different candidates does not appear to have caused any meaningful thermal or mechanical effects on the rod. This crucial finding underscores the value of reducing helium production for IFBA rods. Perhaps future research should broaden the scope to look at boron-free compounds.

The next steps based on the results from this report should be to explore ErB_4 and YbB_6 , with a particular focus on cost, manufacturability and chemical compatibility. A variety of thicknesses should also be explored to confirm that the thickness required to reduce helium production indeed does produce acceptable reactivity suppression.

In conclusion, this research identified ErB_4 and YbB_6 as potential candidates for replacing ZrB_2 in IFBA rods. The neutronics results presented here indicate that similar performance to ZrB_2 can be achieved with less helium production using these compounds. Whilst further research is required to investigate cost, manufacturability and chemical compatibility to ensure no adverse interactions with the fuel or cladding. Alleviating concerns about rod internal pressure for IFBA rods would allow expanded use, extending cycles and improving fuel economics.

6.1 Acknowledgments

First and foremost I would like to thank my supervisors Kyle Johnsson and Zsolt Elter from Westinghouse for their continual support and guidance during the course of this project. Kyle's knowledge of fuel materials and IFBA were instrumental in planning the project and tuning the rod parameters in Transuranus. Zsolt's guidance on neutronics and depletion calculations were very valuable. Additionally, I'd like to thank Paul Blair from Vattenfall for his help in troubleshooting the fission gas release behaviour in Transuranus.

Finally, I would also like to thank my subject reader Vikram Rathore from Uppsala University, as well as Peter Andersson. For giving me a place to work and providing guidance along the way.

Bibliography

- [1] T. Abe and K. Asakura. ‘2.15 - Uranium Oxide and MOX Production’. In: *Comprehensive Nuclear Materials*. Ed. by Rudy J.M. Konings. Oxford: Elsevier, 2012, pp. 393–422. ISBN: 978-0-08-056033-5. DOI: <https://doi.org/10.1016/B978-0-08-056033-5.00036-7>. URL: <https://www.sciencedirect.com/science/article/pii/B9780080560335000367>.
- [2] D.A. Brown, M.B. Chadwick, R. Capote et al. ‘ENDF/B-VIII.0: The 8th Major Release of the Nuclear Reaction Data Library with CIELO-project Cross Sections, New Standards and Thermal Scattering Data’. In: *Nuclear Data Sheets* 148 (2018). Special Issue on Nuclear Reaction Data, pp. 1–142. ISSN: 0090-3752. DOI: <https://doi.org/10.1016/j.nds.2018.02.001>. URL: <https://www.sciencedirect.com/science/article/pii/S0090375218300206>.
- [3] James T. Cahill and Olivia A. Graeve. ‘Hexaborides: a review of structure, synthesis and processing’. In: *Journal of Materials Research and Technology* 8.6 (2019), pp. 6321–6335. ISSN: 2238-7854. DOI: <https://doi.org/10.1016/j.jmrt.2019.09.041>. URL: <https://www.sciencedirect.com/science/article/pii/S2238785418311062>.
- [4] Clément Ciszak et al. ‘On the origins and the evolution of the fuel-cladding bonding phenomenon in PWR fuel rods’. In: *Journal of Nuclear Materials* 520 (2019), pp. 110–120. ISSN: 0022-3115. DOI: <https://doi.org/10.1016/j.jnucmat.2019.04.015>. URL: <https://www.sciencedirect.com/science/article/pii/S0022311519302752>.
- [5] J.R. Deen and J.L. Snelgrove. ‘Neutronics study of LEU fuel options for the HFR-Petten’. eng. In: Argonne National Lab., IL (USA). United States, 1984.
- [6] James J. Duderstadt and Louis J. Hamilton. *Nuclear reactor analysis*. Literaturangaben. New York [u.a.]: Wiley, 1976. 650 pp. ISBN: 0471223638.
- [7] Jordan A. Evans et al. ‘Burnable absorbers in nuclear reactors – A review’. In: *Nuclear Engineering and Design* 391 (2022), p. 111726. ISSN: 0029-5493. DOI: <https://doi.org/10.1016/j.nucengdes>.

- 2022.111726. URL: <https://www.sciencedirect.com/science/article/pii/S0029549322000802>.
- [8] Amir Hosein Fadaei. ‘Investigation of burnable poisons effects in reactor core design’. In: *Annals of Nuclear Energy* 38.10 (2011), pp. 2238–2246. ISSN: 0306-4549. DOI: <https://doi.org/10.1016/j.anucene.2011.06.005>. URL: <https://www.sciencedirect.com/science/article/pii/S0306454911002167>.
- [9] J.H Frye, J.O Betterton and D.S Easton. ‘Thermodynamic properties of zirconium-cadmium and certain other solid solutions’. In: *Acta Metallurgica* 20.10 (1972), pp. 1183–1195. ISSN: 0001-6160. DOI: [https://doi.org/10.1016/0001-6160\(72\)90167-8](https://doi.org/10.1016/0001-6160(72)90167-8). URL: <https://www.sciencedirect.com/science/article/pii/0001616072901678>.
- [10] M. L. Grossbeck et al. *Development of Improved Burnable Poisons for Commercial Nuclear Power Reactors*. INIS RN: 35022589. 2003.
- [11] Group T-2 Los Alamos National Laboratory. *Fission Neutron Yields*. Accessed 2025-06-05. 2012. URL: <https://t2.lanl.gov/nis/endl/intro22.html>.
- [12] Anubhav Jain et al. ‘The Materials Project: A materials genome approach to accelerating materials innovation’. In: *APL Materials* 1.1 (2013), p. 011002. ISSN: 2166532X. DOI: 10.1063/1.4812323. URL: <http://link.aip.org/link/AMPADS/v1/i1/p011002/s1&Agg=doi>.
- [13] Andrew Johnson et al. *serpentTools: A Python Package for Expediting Analysis with Serpent*. 2020. DOI: 10.1080/00295639.2020.1723992.
- [14] C. Josey, B. Forget and K. Smith. ‘High order methods for the integration of the Bateman equations and other problems of the form of $yp=F(y,t)y$ ’. In: *Journal of Computational Physics* 350 (2017), pp. 296–313. ISSN: 0021-9991. DOI: <https://doi.org/10.1016/j.jcp.2017.08.025>. URL: <https://www.sciencedirect.com/science/article/pii/S002199911730596X>.
- [15] Giovanni Laranjo de Stefani et al. ‘Detailed neutronic calculations of the AP1000 reactor core with the Serpent code’. In: *Progress in Nuclear Energy* 116 (2019), pp. 95–107. ISSN: 0149-1970. DOI: <https://doi.org/10.1016/j.pnucene.2019.03.030>. URL: <https://www.sciencedirect.com/science/article/pii/S0149197019300964>.
- [16] Jaakko Leppänen. ‘Development of a new Monte Carlo reactor physics code’. PhD thesis. Finland: Aalto University, 2007, p. 228. ISBN: 9789513870188.
- [17] J. S. Lilley. *Nuclear physics : principles and applications*. eng. The Manchester physics series. Chichester: Wiley, 2001. ISBN: 9780471979364.

- [18] R Manzel and C.T Walker. ‘EPMA and SEM of fuel samples from PWR rods with an average burn-up of around 100 MWd/kgHM’. In: *Journal of Nuclear Materials* 301.2 (2002), pp. 170–182. ISSN: 0022-3115. DOI: [https://doi.org/10.1016/S0022-3115\(01\)00753-X](https://doi.org/10.1016/S0022-3115(01)00753-X). URL: <https://www.sciencedirect.com/science/article/pii/S002231150100753X>.
- [19] Joel McElrath and Keith Fruzzetti. *EPRI PWR primary water chemistry guidelines*. 2014.
- [20] Ignas Mickus. ‘Towards Efficient Monte Carlo Calculations in Reactor Physics: Criticality, Kinetics and Burnup Problems’. PhD thesis. KTH Royal Institute of Technology, 2021.
- [21] Simon C. Middleburgh et al. ‘Atomic Scale Modeling of Point Defects in Zirconium Diboride’. In: *Journal of the American Ceramic Society* 94.7 (Mar. 2011), pp. 2225–2229. ISSN: 1551-2916. DOI: 10.1111/j.1551-2916.2010.04360.x.
- [22] NIST. *Neutron Scattering Lengths List*. <https://www.nist.gov/ncnr/neutron-scattering-lengths-list> (Accessed 2025-06-24).
- [23] J. Noirot et al. ‘Fission gas release behaviour of a 103GWd/tHM fuel disc during a 1200°C annealing test’. In: *Journal of Nuclear Materials* 446.1 (2014), pp. 163–171. ISSN: 0022-3115. DOI: <https://doi.org/10.1016/j.jnucmat.2013.12.002>. URL: <https://www.sciencedirect.com/science/article/pii/S0022311513012889>.
- [24] OECD. *Working Group on Fuel Safety. Report on Fuel Fragmentation, Relocation, Dispersal*. Tech. rep. 2016.
- [25] S. Phapale, R. Mishra and D. Das. ‘Standard enthalpy of formation of compounds of the Cd–Zr system’. In: *Journal of Nuclear Materials* 375.2 (2008), pp. 259–262. ISSN: 0022-3115. DOI: <https://doi.org/10.1016/j.jnucmat.2008.01.004>. URL: <https://www.sciencedirect.com/science/article/pii/S0022311508000196>.
- [26] J. Rest et al. ‘Fission gas release from UO₂ nuclear fuel: A review’. In: *Journal of Nuclear Materials* 513 (2019), pp. 310–345. ISSN: 0022-3115. DOI: <https://doi.org/10.1016/j.jnucmat.2018.08.019>. URL: <https://www.sciencedirect.com/science/article/pii/S0022311518309449>.
- [27] Hannah Ritchie and Pablo Rosado. ‘Electricity Mix’. In: *Our World in Data* (2020). <https://ourworldindata.org/electricity-mix>.
- [28] Randy L. Simmons et al. ‘Integral Fuel Burnable Absorbers with ZrB₂ in Pressurized Water Reactors’. In: *Nuclear Technology* 80.3 (Mar. 1988), pp. 343–348. ISSN: 1943-7471. DOI: 10.13182/nt88-a34058.

- [29] Weston M. Stacey. *Nuclear reactor physics*. Physics Textbook. im Anh.: Errata "Nuclear Reactor Physics" by Weston M. Stacey. Weinheim [u.a.]: Wiley-VCH, 2004. 707 pp. ISBN: 9780471391272.
- [30] K. Takahashi et al. 'Neutron-scattering study of DyB6'. In: *Journal of Magnetism and Magnetic Materials* 177-181 (1998). International Conference on Magnetism (Part II), pp. 1097–1098. ISSN: 0304-8853. DOI: [https://doi.org/10.1016/S0304-8853\(97\)00968-2](https://doi.org/10.1016/S0304-8853(97)00968-2). URL: <https://www.sciencedirect.com/science/article/pii/S0304885397009682>.
- [31] Westinghouse. *Integral Fuel Burnable Absorber (IFBA) Fuel Cycles and IFBA/Gad Hybrid Fuel Cycles*. <https://westinghousenuclear.com/data-sheet-library/integral-fuel-burnable-absorber-ifba-fuel-cycles-and-ifbagad-hybrid-fuel-cycles/> (Accessed 2025-03-15).
- [32] Wikipedia. *Fission chain reaction*. https://commons.wikimedia.org/wiki/File:Fission_chain_reaction.svg (Accessed 2025-06-05).
- [33] Hongxing Xiao, Chongsheng Long and Hongsheng Chen. 'The formation mechanisms of high burnup structure in UO₂ fuel'. In: *Journal of Nuclear Materials* 556 (Dec. 2021), p. 153151. ISSN: 0022-3115. DOI: 10.1016/j.jnucmat.2021.153151.
- [34] Yanchun Zhou et al. 'Theoretical prediction, preparation, and mechanical properties of YbB₆, a candidate interphase material for future UHTCf/UHTC composites'. In: *Journal of the European Ceramic Society* 36.15 (2016). Preparation and Application of Ultra-high Temperature Ceramic Matrix Composites, pp. 3571–3579. ISSN: 0955-2219. DOI: <https://doi.org/10.1016/j.jeurceramsoc.2016.02.053>. URL: <https://www.sciencedirect.com/science/article/pii/S0955221916301030>.

Appendix A

Appendix

The appendix contains a couple of additional plots which may prove useful for future studies based on this work, but which were not used for the present comparison.

A.1 Total Fission Rate

In figure A.1 the total fission rate as a function of radius is shown at various burnup values for the stronger absorbers, and in figure A.2 for the weaker absorbers.

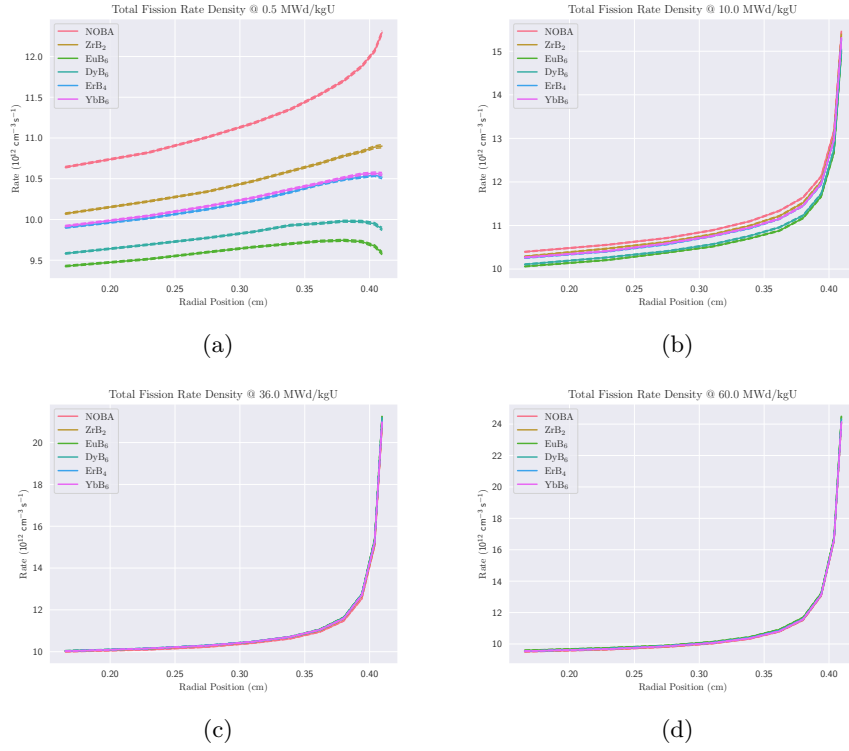


Figure A.1: The figures show the total fission rate density as a function of radius at 0.5, 10.0, 36.0 and 60.0 MWd/kgU for the weaker absorbers.

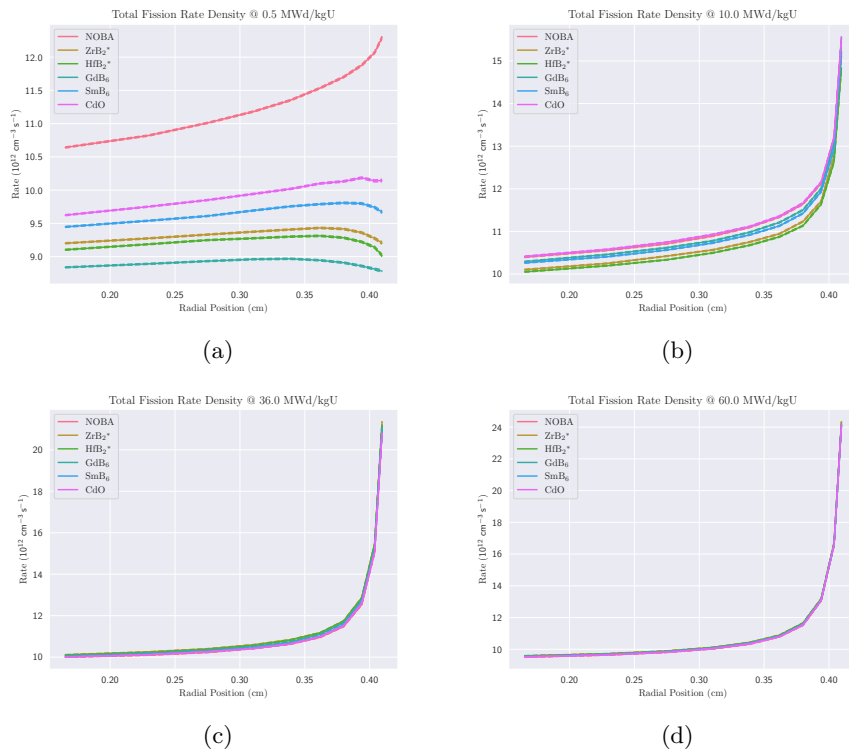


Figure A.2: The figures show the total fission rate density as a function of radius at 0.5, 10.0, 36.0 and 60.0 MWd/kgU for the stronger absorbers.

A.2 Uranium-235 Fission Rate

In figure A.3 the uranium-235 fission rate as a function of radius is shown at various burnup values for the stronger absorbers, and in figure A.4 for the weaker absorbers.

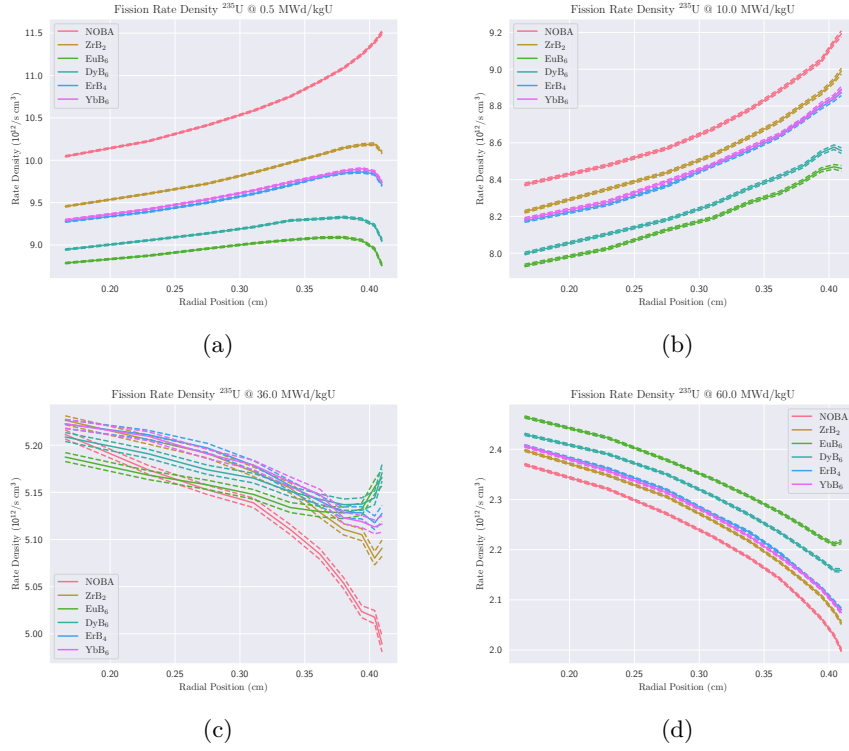


Figure A.3: The figures show the uranium-235 fission rate density as a function of radius at 0.5, 10.0, 36.0 and 60.0 MWd/kgU for the weaker absorbers.

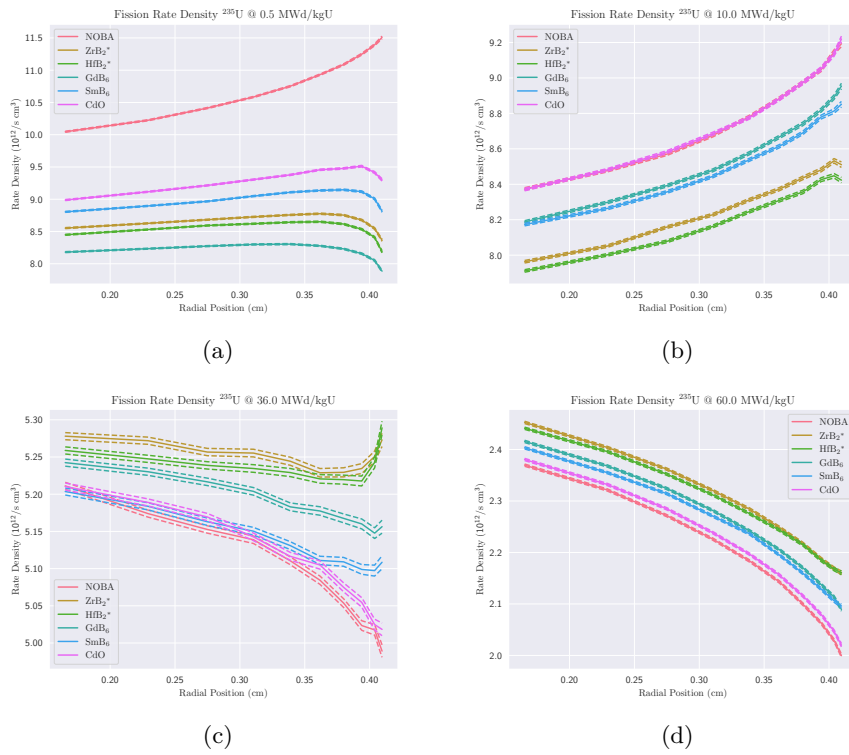


Figure A.4: The figures show the uranium-235 fission rate density as a function of radius at 0.5, 10.0, 36.0 and 60.0 MWd/kgU for the stronger absorbers.

A.3 Uranium-238 Capture Rate

In figure A.6 the uranium-238 capture rate as a function of radius is shown at various burnup values for the stronger absorbers, and in figure A.4 for the weaker absorbers.

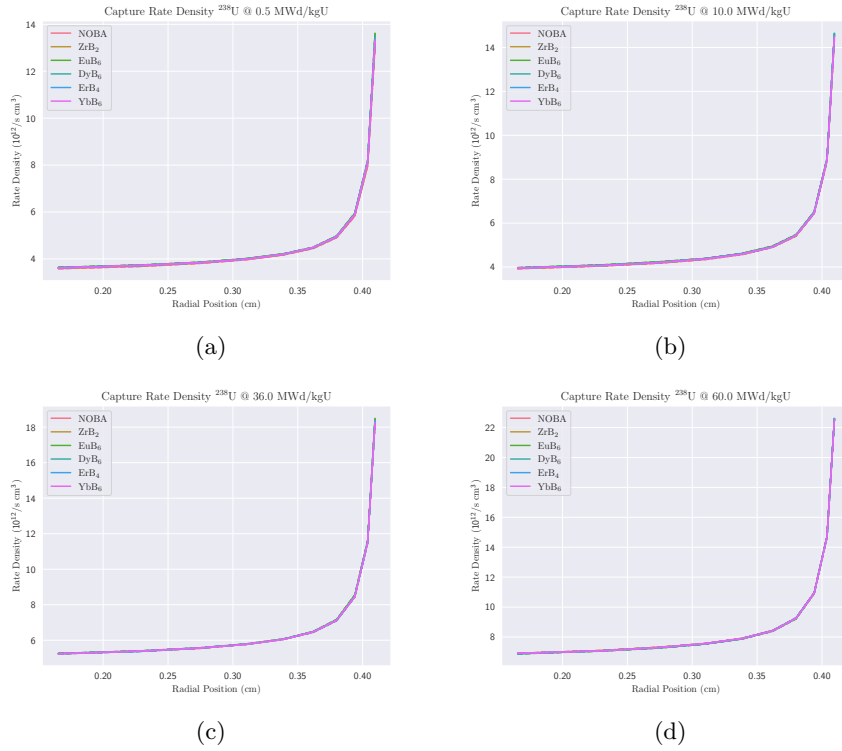


Figure A.5: The figures show the uranium-238 capture rate as a function of radius at 0.5, 10.0, 36.0 and 60.0 MWd/kgU for the weaker absorbers.

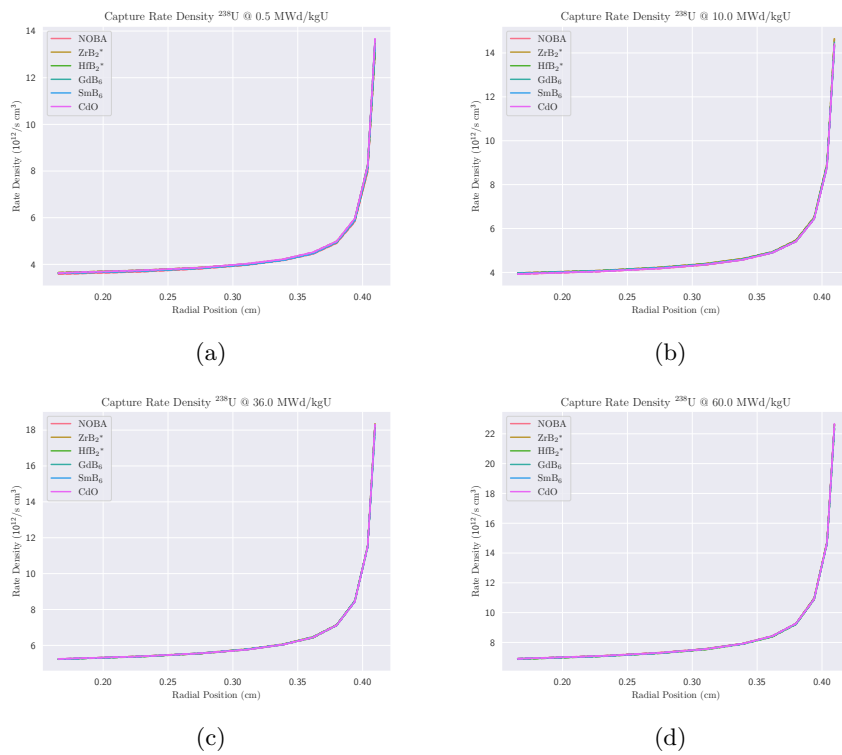


Figure A.6: The figures show the uranium-238 capture rate as a function of radius at 0.5, 10.0, 36.0 and 60.0 MWd/kgU for the stronger absorbers.